AD-A159 348 THEORY AND CALCULATION FOR THE EFFECT OF A HOMOGENEOUS CYLINDRICALLY SYMM..(U) NAVAL OCEAN SYSTEMS CENTER SAN DIEGO CA R A PAPPERT JUL 85 NOSC/TR-1043 1/1

UNCLASSIFIED F/G 20/14 NL

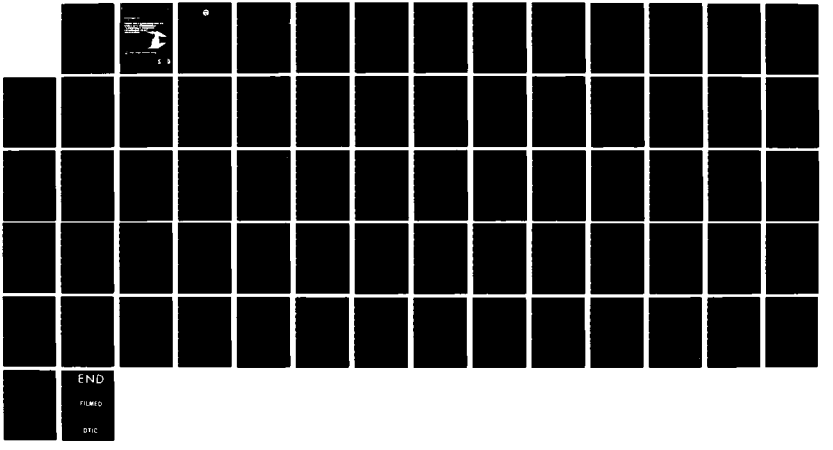

END

FILMED

DTIC

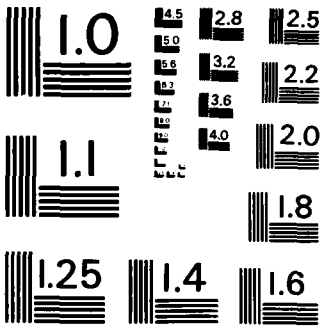

MICROCOPY RESOLUTION TEST CHART
NATIONAL BUREAU OF STANDARDS - 1963 - A

AD-A159 348

THEORY AND CALCULATIONS FOR THE EFFECTS OF A NUCLEAR EXPLOSION ON THE IONOSPHERE AND PROPAGATION

R. A. Pappert

Prepared for
Defense Nuclear Agency

Naval Ocean Systems Center
San Diego, California 92152-5000

Approved for public release; distribution unlimited

DTIC FILE COPY

DTIC ELECTE SEP 18 1985 S D A

85 09 18 020

NAVAL OCEAN SYSTEMS CENTER SAN DIEGO, CA 92152

F. M. PESTORIUS, CAPT, USN
Commander

R.M. HILLYER
Technical Director

ADMINISTRATIVE INFORMATION

This work, sponsored by the Defense Nuclear Agency, was performed during the period December 1984 through July 1985.

Released by
J.A. Ferguson, Head
Modeling Branch

Under authority of
J.H. Richter, Head
Ocean and Atmospheric
Sciences Division

ACKNOWLEDGEMENTS

The author wishes to express his gratitude to Ms. L.R. Hitney for valuable assistance with the computer program implementation of the formulas in Section II.

AS

UNCLASSIFIED
SECURITY CLASSIFICATION OF THIS PAGE

AD A 159 348

(1)

REPORT DOCUMENTATION PAGE

1a REPORT SECURITY CLASSIFICATION UNCLASSIFIED	1b RESTRICTIVE MARKINGS
2a SECURITY CLASSIFICATION AUTHORITY	3 DISTRIBUTION/AVAILABILITY OF REPORT Approved for public release; distribution unlimited.
2b DECLASSIFICATION/DOWNGRADING SCHEDULE	
4 PERFORMING ORGANIZATION REPORT NUMBER(S) NOSC TR 1043	5 MONITORING ORGANIZATION REPORT NUMBER(S)
6a NAME OF PERFORMING ORGANIZATION Naval Ocean Systems Center 6b OFFICE SYMBOL (If applicable)	7a NAME OF MONITORING ORGANIZATION
6c ADDRESS (City, State and ZIP Code) San Diego, CA 92152-5000	7b ADDRESS (City, State and ZIP Code)
8a NAME OF FUNDING/SPONSORING ORGANIZATION Defense Nuclear Agency 8b OFFICE SYMBOL (If applicable)	9 PROCUREMENT INSTRUMENT IDENTIFICATION NUMBER
8c ADDRESS (City, State and ZIP Code) Washington, DC 20350	10 SOURCE OF FUNDING NUMBERS PROGRAM ELEMENT NO: 62715H; PROJECT NO: 99QMXBB; TASK NO:; Agency Accession: DN651 524

11 TITLE (Include Security Classification)
THEORY AND CALCULATION FOR THE EFFECT OF A HOMOGENEOUS, CYLINDRICALLY SYMMETRIC DISTURBANCE ON ELF PROPAGATION

12 PERSONAL AUTHOR(S)
R.A. Pappert

13a TYPE OF REPORT	13b TIME COVERED	14 DATE OF REPORT (Year, Month, Day)	15 PAGE COUNT
Research	FROM Dec 84 TO Jul 85	July 1985	62

16 SUPPLEMENTARY NOTATION

17 COSATI CODES			18 SUBJECT TERMS (Continue on reverse if necessary and identify by block number)
FIELD	GROUP	SUB-GROUP	ELF; VLF; Earth ionosphere waveguide; Ionospheric propagation; Propagation modeling

19 ABSTRACT (Continue on reverse if necessary and identify by block number)

A simple surface propagation model is commonly used to estimate the effects of ionospheric disturbances on extremely low frequency (ELF) propagation. Though often adequate, one shortcoming of the model is its failure to allow for excitation by the broadside component of a horizontal dipole. That excitation can be quite significant in a sporadic-E environment, when the modal polarization can contain a substantial mixture of TE component. In this study a beginning is made on ELF propagation model development which allows for broadside excitation as well as a systematic allowance for height gain effects. The development is for a flat earth with a laterally homogeneous, cylindrically symmetric disturbance centered over the transmitter. The method utilizes normal-mode decomposition. Matching equations at the boundary of the disturbance are developed by evaluating height gain integrals, and it is shown that this method is tantamount to simply matching the ground vertical electric and azimuthal magnetic fields at the boundary. Results for a sporadic-E type environment indicate substantial departures from the surface propagation model and WKB predictions.

20 DISTRIBUTION/AVAILABILITY OF ABSTRACT	21 ABSTRACT SECURITY CLASSIFICATION
[X] UNCLASSIFIED/UNLIMITED [ ] SAME AS RPT [ ] DTIC USERS	UNCLASSIFIED

22a NAME OF RESPONSIBLE INDIVIDUAL	22b TELEPHONE (Include Area Code)	22c OFFICE SYMBOL
R.A. Pappert	(819) 225-7677	Code 544

DD FORM 1473, 84 JAN

83 APR EDITION MAY BE USED UNTIL EXHAUSTED
ALL OTHER EDITIONS ARE OBSOLETE

UNCLASSIFIED
SECURITY CLASSIFICATION OF THIS PAGE

CONTENTS

A1

I. INTRODUCTION

Since an ELF signal from a remote transmitter is received over a range of azimuth angles, lateral ionospheric gradients produced by sporadic-E layering or nuclear depressions can produce significant effects on propagation in the lower ELF band. This is because the Fresnel zone size can be comparable to the transverse dimensions over which the disturbed ionosphere changes significantly. Although a number of workers have addressed the question of propagation in waveguide environments which vary both along and transverse to the path of propagation [Wait, 1964; Greifinger and Greifinger, 1977; Field and Joiner, 1979, 1982; Pappert, 1980, 1985; Ferguson, Hitney and Pappert, 1982; Shellman, 1983], no formulation exists which can fully account for the propagation effects produced by a localized disturbance with simultaneous allowance for vertical inhomogeneity, and anisotropy in a spherical geometry. Thus, it has been common practice to estimate the effects produced by localized ionospheric disturbances by using a simple surface propagation model introduced by Wait and more fully developed by the Greifingers and Field. The theory is predicated on the assumption that the field can be separated into lateral and height-dependent factors, and the model has been used to estimate the behavior of the lateral factor. Excitation factor and height gain effects are generally ignored. When applying the method to nocturnal environments, additional assumptions are made. Among these is the omission of the TE component of the modal polarization. This omission is well justified in the ambient case. However, it is known that under sporadic-E layering, considerable mixing between TE and TM waves can occur. When the surface propagation model is applied to nocturnal sporadic-E environments, this TE component is neglected.

In this study a start is made on ELF propagation model development which allows for the inclusion of excitation-factor and height gain effects along with allowance for the TE component. The development is for a flat earth with a homogeneous, cylindrically symmetric disturbance centered over the transmitter (see Figure 1). The method can be extended to more complicated geometries by methods discussed by the Greifingers and recently implemented by Pappert [1985] for surface model calculations. The development utilizes normal-mode decomposition (only the single non-evanescent mode which propagates at ELF has been used for the calculations), and the normal mode parameters are taken to be independent of the direction or azimuth of propagation. A method akin to mode conversion has been used to develop the matching equations at the boundary, r_0, of the disturbance. This method is shown to be tantamount to simply matching the ground vertical electric and azimuthal magnetic fields at r_0. Results indicate substantial departures from the surface propagation model and WKB predictions.

Essential theoretical background is given in Section II. Azimuthal dependence as well as other features of the modes are discussed in Section III along with the final field results. Conclusions and recommendations are summarized in Section IV.

II. MODEL AND THEORY

The problem is illustrated in Figure 1, where a horizontal electric dipole (current moment Idl) is shown within the earth-ionosphere waveguide and beneath the center of a large cylindrically symmetric patch of sporadic-E. The vertical composition of the nighttime ambient electron and ion profiles with and without the sporadic-E layer is shown in Figure 2. The ground is taken to be homogeneous, with conductivity σ_g and permittivity ε_g. A crucial assumption, discussed more fully in Section III, is that the propagation is independent of its azimuth. The electric, $\vec{E}$, and magnetic, $\vec{H}$, fields excited by the horizontal dipole can be derived from two scalar potentials V and W [Wait, 1963], where V is identified with quasi TM excitation and W with quasi TE excitation. Total field components within the guide are given by [Webber and Peden, 1971].

$$H_z = \left(\frac{\partial^2}{\partial z^2} + k^2\right)W \quad , \qquad E_z = \left(\frac{\partial^2}{\partial z^2} + k^2\right)V \tag{1-a}$$

$$H_\phi = -j\omega\varepsilon_o \frac{\partial V}{\partial r} + \frac{1}{r}\frac{\partial^2 W}{\partial z \partial \phi} \quad , \quad E_\phi = j\omega\mu_o \frac{\partial W}{\partial r} + \frac{1}{r}\frac{\partial^2 V}{\partial r \partial \phi} \tag{1-b}$$

$$H_r = \frac{\partial^2 W}{\partial z \partial r} + \frac{j\omega\varepsilon_o}{r}\frac{\partial V}{\partial \phi} \quad , \quad E_r = \frac{\partial^2 V}{\partial z \partial r} - \frac{j\omega\mu_o}{r}\frac{\partial W}{\partial \phi} \tag{1-c}$$

where ω, μ_o, ε_o and k are angular frequency, free space permeability, free space permittivity and free space wavenumber, respectively. A time dependence $\exp(j\omega t)$ is assumed and $j = \sqrt{-1}$.

Free space field components, E_z^p , and, H_z^p, generated by the horizontal electric dipole are:

$$E_z^p = \pm \frac{Mk^3}{2}\cos\phi \int_\Gamma S^2 CH_1^{(2)}(kSr)\exp(-jkC|z-z_o|)d\theta \tag{2}$$

$$\eta H_z^p = \frac{Mk^3}{2} \sin\phi \int_\Gamma S^2 H_1^{(2)}(kSr)\exp(-jkC|z-z_0|)d\theta \tag{3}$$

where

$$M = Idl/(4\pi j\omega\varepsilon_0) \ , \ S = \sin\Theta \ , \ C = \cos\Theta \ , \ \eta = \sqrt{\mu_0/\varepsilon_0} \tag{4}$$

Gamma, Γ, is the contour with lower endpoint $-\pi/2-j\infty$ and upper endpoint $\pi/2+j\infty$. $H_1^{(2)}$ is the Hankel function of order 1 of the second kind. The plus sign in Eq. (2) applies when $z > z_0$ and the minus sign when $z < z_0$, where z_0 is the transmitter height (see Figure 1).

To the primary field components represented by Eqs. (2) and (3) must be added the field components associated with the boundary reflections or, equivalently, the image fields. Let R be the plane wave reflection matrix, referenced to ground level, associated with reflections from structure above z_0 and $\bar{R}$ the corresponding reflection matrix associated with reflections from structure below z_0. In terms of the elements defined by Budden [1961], the reflection matrices associated with the z field components are:

$$R = \begin{pmatrix} {}_{\parallel}R_{\parallel} & -{}_{\perp}R_{\parallel} \\ -{}_{\parallel}R_{\perp} & {}_{\perp}R_{\perp} \end{pmatrix}, \ \bar{R} = \begin{pmatrix} {}_{\parallel}\bar{R}_{\parallel} & 0 \\ 0 & {}_{\perp}\bar{R}_{\perp} \end{pmatrix} \tag{5}$$

The notation $\parallel$ denotes vertical polarization, and the notation $\perp$ denotes horizontal polarization. The first subscript refers to the polarization of the electric field of the upgoing wave while the second subscript refers to the corresponding polarization of the downcoming wave. Following Pappert [1968], the total z field components within the guide may be written as

$$\begin{pmatrix} E_z \\ \eta H_z \end{pmatrix} = \frac{Mk^3}{2}\left[\cos\phi \int_\Gamma S^2 CH_1^{(2)}(kSr)(e^{-jkCz} + Re^{jkCz})F(e^{jkCz_o} - \bar{R}e^{-jkCz_o})\begin{pmatrix}1\\0\end{pmatrix}d\theta \right.$$

$$\left. + \sin\phi \int_\Gamma S^2 H_1^{(2)}(kSr)(e^{-jkCz} + Re^{jkCz})F(e^{jkCz_o} + \bar{R}e^{-jkCz_o})\begin{pmatrix}0\\1\end{pmatrix}d\theta\right] \qquad (6)$$

where

$$F = (1-R\bar{R})^{-1} \qquad (7)$$

By carrying out the matrix operations indicated in Eqs. (6) and (7) and evaluating the integral by means of residue theory [Budden, 1962] one obtains

$$E_z = \pi j Mk^3 \cos\phi \sum_m \left[\frac{S^2 CH_1^{(2)}(kSr)(1-{}_\perp R_\perp \bar{R}_\perp)(e^{jkCz} + {}_\parallel \bar{R}_\parallel e^{-jkCz})(e^{jkCz_o} - {}_\parallel \bar{R}_\parallel e^{-jkCz_o})}{{}_\parallel \bar{R}_\parallel (\partial\Delta/\partial\theta)}\right]_m$$

$$- \pi j Mk^3 \sin\phi \sum_m \left[\frac{S^2 H_1^{(2)}(kSr)\,{}_\perp R_\parallel\,(e^{jkCz} + {}_\parallel \bar{R}_\parallel e^{-jkCz})(e^{jkCz_o} + {}_\perp \bar{R}_\perp e^{-jkCz_o})}{\partial\Delta/\partial\theta}\right]_m \qquad (8)$$

$$\eta H_z = -\pi j Mk^3 \cos\phi \sum_m \left[\frac{S^2 CH_1^{(2)}(kSr)\;{}_\parallel R_\perp\,(e^{jkCz} + {}_\perp \bar{R}_\perp e^{-jkCz})(e^{jkCz_o} - {}_\parallel \bar{R}_\parallel e^{-jkCz_o})}{\partial\Delta/\partial\theta}\right]_m$$

$$+ \pi j Mk^3 \sin\phi \sum_m \left[\frac{S^2 H_1^{(2)}(kSr)(1-{}_\parallel R_\parallel {}_\parallel \bar{R}_\parallel)(e^{jkCz} + {}_\perp \bar{R}_\perp e^{-jkCz})(e^{jkCz_o} + {}_\perp \bar{R}_\perp e^{-jkCz_o})}{{}_\perp \bar{R}_\perp (\partial\Delta/\partial\theta)}\right]_m \qquad (9)$$

Here m is a mode index (only one non-evanescent mode exists in the ELF band) and the modal function is

$$\Delta = (1-{}_\parallel R_\parallel {}_\perp \bar{R}_\parallel)(1-{}_\perp R_\perp {}_\perp \bar{R}_\perp) - {}_\perp \bar{R}_\perp {}_\parallel \bar{R}_\parallel {}_\perp R_\parallel {}_\parallel R_\perp \qquad (10)$$

The modal equation $\Delta = 0$ has also been used in arriving at Eqs. (8) and (9).

From Eqs. (1-a) the total potentials V and W within the guide are

$$V = \pi jMk \sum_m \left\{ \frac{H_1^{(2)}(kSr)\left(e^{jkCz_+} {}_{\parallel}\bar{R}_{\parallel}\, e^{-jkCz}\right)}{\partial\Delta/\partial\Theta} \left[\frac{(1 - {}_{\perp}R_{\perp}\, {}_{\perp}\bar{R}_{\perp})C\left(e^{jkCz_o} - {}_{\parallel}\bar{R}_{\parallel} e^{-jkCz_o}\right)}{{}_{\parallel}\bar{R}_{\parallel}} \cos\phi \right.\right.$$

$$\left.\left. - {}_{\perp}R_{\parallel}\left(e^{jkCz_o} + {}_{\perp}\bar{R}_{\perp} e^{-jkCz_o}\right)\sin\phi \right] \right\}_m \qquad (11)$$

$$\eta W = -\pi jMk \sum_m \left\{ \frac{H_1^{(2)}(kSr)\left(e^{jkCz} + {}_{\perp}\bar{R}_{\perp} e^{-jkCz}\right)}{\partial\Delta/\partial\Theta} \left[{}_{\parallel}R_{\perp} C\left(e^{jkCz_o} - {}_{\parallel}\bar{R}_{\parallel}\, e^{-jkCz_o}\right)\cos\phi \right.\right.$$

$$\left.\left. - \frac{(1 - {}_{\parallel}R_{\parallel}\, {}_{\parallel}\bar{R}_{\parallel})\left(e^{jkCz_o} + {}_{\perp}\bar{R}_{\perp} e^{-jkCz_o}\right)}{{}_{\perp}\bar{R}_{\perp}} \sin\phi \right] \right\}_m \qquad (12)$$

Equations (11) and (12) may be conveniently written as

$$V = -\pi jMk \sum_m \left\{ \lambda H_1^{(2)}(kSr) h_y(z) \left[e_x(z_o)\cos\phi + \alpha e_y(z_o)\sin\phi \right] \right\}_m \qquad (13)$$

$$\eta W = \pi jMk \sum_m \left\{ \lambda H_1^{(2)}(kSr) e_y(z) \left[e_x(z_o)\cos\phi + \alpha e_y(z_o)\sin\phi \right] \right\}_m \qquad (14)$$

where

$$\lambda = \frac{(1 - {}_{\perp}R_{\perp}\, {}_{\perp}\bar{R}_{\perp})(1 + {}_{\parallel}\bar{R}_{\parallel})^2}{{}_{\parallel}\bar{R}_{\parallel}\ (\partial\Delta/\partial\Theta)} \quad , \quad \alpha = \frac{{}_{\perp}R_{\parallel}}{{}_{\parallel}R_{\perp}} \qquad (15)$$

and the modal height gains h_y and e_y are defined by

$$h_y(z) = \frac{e^{jkCz_+} {}_{\parallel}\bar{R}_{\parallel}\, e^{-jkCz}}{1 + {}_{\parallel}R_{\parallel}} \quad , \quad e_y(z) = f\, \frac{e^{jkCz_+} {}_{\perp}\bar{R}_{\perp} e^{-jkCz}}{1 + {}_{\perp}\bar{R}_{\perp}} \qquad (16)$$

All other height gains are given by Maxwell's equations subject to y invariance and an exp(-jkSx) dependence. The other height gains are (note that h is defined as η times the magnetic intensity).

$$e_x = -\frac{1}{jk}\frac{\partial h_y}{\partial z} = -C\frac{e^{jkCz}\,{}_{\parallel}\bar{R}_{\parallel}\;e^{-jkCz}}{1+{}_{\parallel}\bar{R}_{\parallel}}\,,\quad h_x = \frac{1}{jk}\frac{\partial e_y}{\partial z} = fC\,\frac{e^{jkCz}\,{}_{\perp}\bar{R}_{\perp}e^{-jkCz}}{1+{}_{\perp}\bar{R}_{\perp}} \qquad (17)$$

$$e_z = \frac{h_y}{jk\exp(-jkSx)}\frac{\partial}{\partial x}[\exp(-jkSx)] = -Sh_y,\quad h_z = -\frac{e_y}{jk\exp(-jkSx)}\frac{\partial}{\partial x}[\exp(-jkSx)] = Se_y \qquad (18)$$

Because of the assumed propagation isotropy in azimuth, the height gains are independent of the azimuth angle ϕ. In Eqs. (16) and (17), f is the modal polarization ratio given by

$$f = \frac{e_y(z=0)}{h_y(z=0)} = \frac{(1+{}_{\perp}\bar{R}_{\perp})(1-{}_{\parallel}R_{\parallel}\,{}_{\parallel}\bar{R}_{\parallel})}{(1+{}_{\parallel}\bar{R}_{\parallel})\,{}_{\perp}R_{\parallel}\,{}_{\perp}\bar{R}_{\perp}} = \frac{(1+{}_{\perp}\bar{R}_{\perp})}{(1+{}_{\parallel}\bar{R}_{\parallel})}\,\frac{{}_{\parallel}R_{\perp}\,{}_{\parallel}\bar{R}_{\parallel}}{1-{}_{\perp}R_{\perp}\,{}_{\perp}\bar{R}_{\perp}} \qquad (19)$$

Thus far the discussion has been restricted to the region within the guide. The modal height gains, however, have meaning both within and wihout the guide (e.g., within the ionosphere) and are calculable by means of numerical integration of Maxwell's equations [Pitteway, 1965; Smith, 1970]. Therefore, with the understanding that h_y, e_y , etc., represent these general height gain functions, the field components deduced from V and W by means of Eqs. (1) can be continued into the ionosphere.

In anticipation of solving the problem posed in Fig. 1 by satisfying continuity requirements at the boundary $r=r_0$, the superscript p will be used to denote values in the perturbed region, and the superscript u will be used to denote values in the unperturbed region. To the primary fields in the perturbed region must be added the secondary fields. The crucial assumption is now made that these secondary fields generated by the discontinuity at $r = r_0$ may be described in terms of a normal-mode expansion so that the secondary potentials take the form

$$V_s = \sum_m \{J_1(kS^p r)h_y^p(z)(x_1\cos\phi + x_2\sin\phi)\}_m \qquad (20)$$

$$\pi W_s = -\sum_m \{J_1(kS^p r) e_y^p(z)\ (x_1 \cos\phi + x_2 \sin\phi)\}_m \tag{21}$$

where J_1 is the Bessel function of the first kind of order one and guarantees that the secondary fields are finite at the origin. It is likewise assumed that the potentials in the unperturbed region can be written in terms of a normal-mode expansion so that

$$V_e = \sum_m \{H_1^{(2)}(kS^u r) h_y^u(z)(x_3 \cos\phi + x_4 \sin\phi)\}_m \tag{22}$$

$$\pi W_e = -\sum_m \{H_1^{(2)}(kS^u r) e_y^u(z)(x_3 \cos\phi + x_4 \sin\phi)\}_m \tag{23}$$

Matching the tangential components of the fields at $r = r_o$ yields

$$j\pi Mk^3 \sum_m \left\{ \lambda^p S^p [e_x^p(z_o)\cos\phi + \alpha^p e_y^p(z_o)\sin\phi] \begin{bmatrix} jH_1^{(2)'}(kS^p r_o) e_y^p(z) \\ H_1^{(2)}(kS^p r_o) e_z^p(z) \\ jH_1^{(2)'}(kS^p r_o) h_y^p(z) \\ H_1^{(2)}(kS^p r_o) h_z^p(z) \end{bmatrix} \right.$$

$$\left. + j\lambda^p S^p \frac{H_1^{(2)}(kS^p r_o)}{kS^p r_o} [-e_x^p(z_o)\sin\phi + \alpha^p e_y^p(z_o)\cos\phi] \begin{bmatrix} e_x^p(z) \\ 0 \\ h_x^p(z) \\ 0 \end{bmatrix} \right\}_m$$

$$-k^2 \sum_m \left\{ S^p (x_1 \cos\phi + x_2 \sin\phi) \begin{bmatrix} jJ_1'(kS^p r_o) e_y^p(z) \\ J_1(kS^p r_o) e_z^p(z) \\ jJ_1(kS^p r_o) h_y^p(z) \\ J_1(kS^p r_o) h_z^p(z) \end{bmatrix} \right.$$

IV SUMMARY

In this report, a development to allow for the inclusion of excitation factor and height gain effects on ELF propagation in a laterally inhomogeneous guide has been started. The development is for a flat earth geometry and the simple environment of Figure 1. Several crucial assumptions have been made. First, it has been assumed that the perturbing environment is homogeneous as well as cylindrically symmetric. Second, it has been assumed that the primary fields, as well as secondary fields generated by the boundary at $r = r_0$, are described by normal modes, and only the consequences of the single non-evanescent mode have been investigated. Third, the normal-mode parameters have been taken to be independent of the direction or azimuth of propagation.

A method akin to mode conversion, termed in this study the SMA (for Single Mode Analysis) method, has been used for establishing the boundary equations at $r = r_0$. As in mode conversion analysis, the SMA method involves numerical integration of height gain functions. It has been shown that the SMA method is tantamount to matching H_ϕ and E_z at $r = r_0$ at the ground. This is a significant result because it implies the reasonableness of a generalized surface propagation model which allows in a systematic way for excitation factor and height gain effects as well as broadside excitation.

It has been found that excitation factor and height gain effects can be quite significant for sporadic-E environments conforming to the geometry of Figure 1. In particular, broadside excitation, because of the sizable TE contamination of the modal polarization, can be very substantial. TE contamination would also be expected to play a role were the disturbance to fall over the receiver rather than over the transmitter.

the dominating terms of Eqs. (29) through (32) involve integrals of products of e_z and h_y terms. These terms are nearly constant and of order unity below about 73 km (see Figures 29 and 30), where most of the contribution to the integrals comes from. The integrals involving the products of TE components would generally be much smaller, as Figures 29 and 30 show. At any rate, it is a fact that *simply matching the* H_ϕ *and* E_z *components at* $r = r_o$ at the ground is for all practical purposes equivalent to the height gain integration method (the SMA method) used in Section II to develop the results. This is made clear in Figures 31 through 34, which show a worst-case comparison between SMA results and "Field Matching" results (i.e., results obtained by demanding continuity of H_ϕ and E_z at the ground at $r = r_o$). The differences are indeed very slight. This is a significant result because it implies the reasonableness of a generalized surface propagation model which allows in a systematic way for excitation factor and height gain effects as well as broadside excitation.

A disquieting though not surprising feature of the analysis is that the TE components are not continuous at $r = r_o$. This would be expected for the E_ϕ and H_z components since, as Figures 29 and 30 show, e_y and h_z vary substantially across the guide. However, the h_x component is quite substantial and reasonably stable across the guide. But as Figure 35 (a representative example) shows, the H_r component experiences a large discontinuity at $r = r_o$ at the ground. This is not surprising because, as we have just seen, the SMA method is equivalent to matching only the H_ϕ and E_z components at $r = r_o$ at the ground. It is not clear what the resolution to this dilemma is. Perhaps inclusion of evanescent modes would improve the agreement for continuity of H_r without destroying the H_ϕ and E_z continuity. However, no efforts along those lines have been attempted in the current study.

close to broadside, excitation variation for the unperturbed guide is close to the surface model result; however, the perturbed guide's normalized source height gain variation shows marked departure from the surface model result. This is because of the large TE admixture to the modal polarization in the perturbed region. Whereas for the unperturbed guide $|e_x^u(o)| >> |e_y^u(o)|$, the situation for the perturbed guide is that $|e_y^p(o)|$ is somewhat greater than $|e_x^p(o)|$, and that results in the interference null in Figure 16 occurring at $\simeq 36°$ and for the region $\phi < 0$ being essentially a region of constructive interference.

Figures 17 and 18 show results for the amplitude radios $|H_\phi/H_\phi^u|$ and $|E_z/E_z^u|$ at the ground for crossed dipole sources which are out of phase by 90°. Shown are SMA, WKB and surface propagation model results. Again the SMA results are very nearly continuous at $r = r_o$ while the WKB results manifest sizable discontinuities there. Exterior to the disturbance, the SMA and surface propagation model results are in reasonable agreement. Interior to the disturbance, the SMA results for H_ϕ differ significantly from the surface propagation model results while the interior results for E_z for the two models are in reasonable agreement.

Figures 19 through 28 show SMA and WKB phase results for H_ϕ and E_z for the cases for which amplitude results have been given previously. The significant features are the near continuity of the phase of H_ϕ and E_z at $r = r_o$ for the SMA method and the large discontinuity exhibited there by the WKB results. The near continuity of the amplitudes and phases at $r = r_o$ means that the height gain integration method used in Section II to develop the results is tantamount to simply matching H_ϕ and E_z components at $r = r_o$ at the ground. The latter method involves no height gain integrations such as used in the method of Section II. It is suspected that the reason for this is that

iii) SMA results show significant departures from both the surface propagation model and the WKB results.

iv) At short ranges the SMA and WKB results generally show good agreement.

v) In contrast to the surface propagation model results, the SMA results show a marked angular (i.e., ϕ) dependence.

Result (i) above is due in large measure to the large discrepancy between the perturbed (θ^p= 57.16° - 65.03°j) and unperturbed (θ^u = 84.48° - 34.12°j) eigenangles as well as the difference between the perturbed [$e_y^p(o)$ = (5.78 - 6.77j)x10^{-4}] and unperturbed [$e_y^u(o)$ = (5.25-2.21j)x10^{-5}] field components and the difference between the excitation factors (λ^p = 2.32 - 4.99j and λ^u = - 4.82x10^{-2} - 7.42j). In connection with (ii) above, it is pointed out that continuity of the field components H_ϕ and E_z is not obviously forced by the matching method of Section II. Departures mentioned in (iii) point out clearly the significance of height gain and excitation factor effects ignored in the surface propagation model. Observation (iv) is explained by the fact that the secondary fields [which depend upon $J_1(kS^pr)$ and $J_1'(kS^pr)$] for $|kS^pr|<<1$ are small compared with the primary fields which depend upon $H_1^{(2)}(kS^pr)$ and $H_1^{(2)'}(kS^pr)$. Figure 16 illustrates the source of the angular dependence mentioned in (v). Shown is the normalized source height gain $(e_x(o)\cos\phi + e_y(o)\sin\phi)/e_x(o)$ in dB for both the perturbed "p" and unperturbed "u" quantities versus azimuth. Shown also is the $20\log_{10}|\cos\phi|$ variation predicted by the surface propagation model (which assumes only excitation from the end-on component of the source dipole). Except for angles

vertical component of the geomagnetic field for high latitudes. Azimuthal invariance is strictly valid for a dip angle of 90°.

All remaining figures in this study are for 75 Hz, and for a vertical geomagnetic field (i.e., dip of 90°) of strength .41 x sin(77°) gauss. The ground conductivity has been taken to be 10^{-2} siemens/m and the dielectric constant 15. The lower conductivity of about 2.8×10^{-4} siemens/m at the transmitter can be included by simply multiplying the height gains $e_x^p(p)$ and $e_y^p(o)$ by $\sqrt{10^{-2}/2.8 \times 10^{-4}} = 5.98$ (or 15.5 dB). However, the factor is of no consequence in the present study, where either amplitude ratios or phase differences are plotted. Finally, the radius of the disturbance has been taken to be 500 km.

Figures 8 through 15 show results for the amplitude ratios $|H_\phi/H_\phi^u|$ and $|E_z/E_z^u|$ at the ground for an electric dipole source at the ground oriented in the x direction (see Figure 1). Figures 8 and 9 are for broadside launch (i.e., $\phi = \pm 90°$), Figures 10 and 11 are for $\phi = 45°$, Figures 12 and 13 are for end-on launch (i.e., $\phi = 0°$), and Figures 14 and 15 are for $\phi = -45°$. Results of the present study are labeled SMA for Single Mode Analysis. Shown also on Figures 10 through 15 are WKB results and results of the surface propagation model, which neglects excitation factor and height gain effects (Pappert, 1985). The surface propagation results are ϕ independent. There are several observations that can be made from these figures.

i) WKB results generally show a sizable discontinuity at $r = r_o$.

ii) SMA results are very nearly continuous at $r = r_o$ though range derivatives are discontinuous.

ELF propagation in the ambient guide can be taken to be independent of azimuth.

Figure 5 shows that the azimuthal deviation from the average attenuation rate for the disturbed profile (i.e., ambient plus sporadic-E) is less than 10%. The large difference between the mean attenuation rates for the two dips shown on Figure 5 results from the critical role which the vertical component of the geomagnetic field plays in determining the attenuation rate. This is discussed in the work of Pappert and Moler [1978]. Possible contributions of this effect to azimuthal variations as well as azimuthal dependence due to possible lateral inhomogneity of the layer are ignored in this study. Finally, Figure 6 shows that the azimuthal deviation from the average normalized phase velocity for the disturbed profile is also less than 10%. Thus, though the evidence for assuming azimuthally independent propagation in this instance is not as formidable as in the case of the ambient profile, the azimuthal variations for constant dip angle are still sufficiently small to make reasonable, at least as a first approximation, the assumption of azimuthal invariance. The assumption is, of course, most reasonable when applied to effects caused by natural or artificial ionospheric depressions and has served as the basis for the theoretical development of Section II.

Figure 7 shows attenuation rate as a function of frequency for the ambient nighttime profile and the ambient plus sporadic-E profile. Two curves for the disturbed environment are shown. The solid curve is for a dip angle of 77°, a geomagnetic field strength of 0.41 gauss, a ground conductivity of 10^{-2} siemens/m and dielectric constant of 15. The dashed curve is for a dip of 90° and a geomagnetic field strength of 0.41 x sin(77°) gauss (i.e., the radial component of the geomagnetic field used for the solid curve). The near coincidence of the two curves demonstrates the controlling feature of the

III. RESULTS

In a previous study [Pappert and Moler, 1978] full-wave outputs for an ambient nighttime profile disturbed by a sporadic-E layer (see Figure 2) have been analyzed with respect to ionospheric absorption and reflection features at lower ELF. In that work it was shown that an order-of-magnitude enhancement in the attenuation rate due to the sporadic-E layering was a distinct possibility (see also Figures 3, 5 and 7 herein). In this section, features of the propagation associated with the simple sporadic-E environment of Figures 1 and 2 will be explored by implementation of theory developed in Section II.

Figures 3 through 6 show the behavior of the attenuation rate and phase velocity (normalized to the free space speed of light) at 75 Hz as a function of azimuth of propagation relative to magnetic north for dip angles of 60° and 75°. A conductivity of $\sigma = 10^{-2}$ siemens/m, dielectric constant of 15, and geomagnetic field strength of 0.41 gauss have been used for the calculations. Figure 3 indicates mid and northerly latitude ambient attenuation rates of slightly greater than 0.8 dB/Mm. This is somewhat lower than the WTF measurements, which estimate a nighttime mid-latitude value of 1.0 dB/Mm. This comparison could be indicative of a deficiency in the ionospheric model, although other models also generally yield lower attenuation rates than those suggested by WTF measurements. Most measurements of ELF nocturnal fades have been made for paths for which the dip angle is $\lesssim 60°$. The curves of Figure 3 indicate an azimuthal variation in attenuation rate of less than 0.03 dB/Mm. Similarly, Figure 4 shows the difference in the normalized phase velocity for the east to west and west to east directions is less than 1%. Thus, for paths of concern in this study,

$$
\left.
\begin{aligned}
\pi H_{\phi}^{w} &= -\pi M k^{3} \sum_{m} \Bigg\{ \lambda_{m}^{p} S_{m}^{p} H_{1}^{(2)'}(kS_{m}^{p}r) h_{ym}^{p}(z) \left[e_{xm}^{p}(z_{o})\cos\phi + \alpha_{m}^{p} e_{ym}^{p}(z_{o})\sin\phi \right] \\
&\quad + \lambda_{m}^{p} S_{m}^{p} \frac{H_{1}^{(2)}(kS_{m}^{p}r)}{kS_{m}^{p}r} h_{xm}^{p}(z) \left[-e_{xm}^{p}(z_{o})\sin\phi + \alpha_{m}^{p} e_{ym}^{p}(z_{o})\cos\phi \right] \Bigg\} \qquad , \quad r<r_{o} \\
&= -\pi M k^{3} \sum_{m} \Bigg\{ \sqrt{\lambda_{m}^{p}\lambda_{m}^{u}}\, \bar{S}_{m} H_{1}^{(2)'}(k\bar{S}_{m}r) h_{ym}^{u}(z) \left[e_{xm}^{p}(z_{o})\cos\phi + \alpha_{m}^{p} e_{ym}^{p}(z_{o})\sin\phi \right] \\
&\quad + \sqrt{\lambda_{m}^{p}\lambda_{m}^{u}}\, \bar{S}_{m} \frac{H_{1}^{(2)}(k\bar{S}_{m}r)}{k\bar{S}_{m}r} h_{xm}^{u}(z) \left[-e_{xm}^{p}(z_{o})\sin\phi + \alpha_{m}^{p} e_{ym}^{p}(z_{o})\cos\phi \right] \Bigg\} \qquad , \quad r>r_{o}
\end{aligned}
\right\} \tag{40}
$$

$$
\left.
\begin{aligned}
\pi H_{r}^{w} &= -\pi M k^{3} \sum_{m} \Bigg\{ \lambda_{m}^{p} S_{m}^{p} H_{1}^{(2)'}(kS_{m}^{p}r) h_{xm}^{p}(z) \left[e_{x}^{p}(z_{o})\cos\phi + \alpha_{m}^{p} e_{ym}^{p}(z_{o})\sin\phi \right] \\
&\quad - \lambda_{m}^{p} S_{m}^{p} \frac{H_{1}^{(2)}(kS_{m}^{p}r)}{kS_{m}^{p}r} h_{ym}^{p}(z) \left[-e_{xm}^{p}(z_{o})\cos\phi + \alpha_{m}^{p} e_{ym}^{p}(z_{o})\sin\phi \right] \Bigg\} \qquad , \quad r<r_{o} \\
&= -\pi M k^{3} \sum_{m} \Bigg\{ \sqrt{\lambda_{m}^{p}\lambda_{m}^{u}}\, \bar{S}_{m} H_{1}^{(2)'}(k\bar{S}_{m}r) h_{xm}^{u}(z) \left[e_{xm}^{p}(z_{o})\cos\phi + \alpha_{m}^{p} e_{ym}^{p}(z_{o})\sin\phi \right] \\
&\quad - \sqrt{\lambda_{m}^{p}\lambda_{m}^{u}}\, \bar{S}_{m} \frac{H_{1}^{(2)}(k\bar{S}_{m}r)}{k\bar{S}_{m}r} h_{ym}^{u}(z) \left[-e_{xm}^{p}(z_{o})\cos\phi + \alpha_{m}^{p} e_{ym}^{p}(z_{o})\sin\phi \right] \Bigg\} \qquad , \quad r>r_{o}
\end{aligned}
\right\} \tag{41}
$$

where

$$
\bar{S}_{m} = \frac{S_{m}^{p} r_{o} + S_{m}^{u}(r-r_{o})}{r} \qquad , \quad r>r_{o} \tag{42}
$$

Results based on Eqs. (33) through (41) are given in the following section.

$$E_z^u = j\pi Mk^3 \sum_m \lambda_m^u S_m^u H_1^{(2)}(kS_m^u r) e_{zm}^u(z) [e_{xm}^u(z_o)\cos\phi + \alpha_m^u e_{ym}^u(z_o)\sin\phi] \tag{36}$$

$$\pi H_\phi^u = -\pi Mk^3 \sum_m \left\{ \lambda_m^u S_m^u \, H_1^{(2)'}(kS_m^u r) h_{ym}^u(z) [e_{xm}^u(z_o)\cos\phi + \alpha_m^u e_{ym}^u(z_o)\sin\phi] \right.$$

$$\left. + \lambda_m^u S_m^u \frac{H_1^{(2)}(kS_m^u r)}{kS_m^u r} h_{xm}^u(z) [-e_{xm}^u(z_o)\sin\phi + \alpha_m^u e_{ym}^u(z_o)\cos\phi] \right\} \tag{37}$$

$$\pi H_r^u = -\pi Mk^3 \sum_m \left\{ \lambda_m^u S_m^u \, H_1^{(2)'}(kS_m^u r) h_{xm}^u(z) [e_{xm}^u(z_o)\cos\phi + \alpha_m^u e_{ym}^u(z_o)\sin\phi] \right.$$

$$\left. - \lambda_m^u S_m^u \frac{H_1^{(2)}(kS_m^u r)}{kS_m^u r} h_{ym}^u(z) [-e_{xm}^u(z_o)\sin\phi + \alpha_m^u e_{ym}^u(z_o)\cos\phi] \right\} \tag{38}$$

As a matter of interest, comparisons will also be made in the following section with the so-called WKB result [Bickel et al., 1970] which involves the geometric mean of the excitation factor at the terminals of the path and the average of the propagation constant over the path. The WKB formulas for the field as implemented in the present study are as follows:

$$\left. \begin{aligned} E_z^w &= j\pi Mk^3 \sum_m \lambda_m^p S_m^p \, H_1^{(2)}(kS_m^p r) e_{zm}^p(z) [e_{xm}^p(z_o)\cos\phi + \alpha_m^p e_{ym}^p(z_o)\sin\phi] \quad , \quad r<r_o \\ &= j\pi Mk^3 \sum_m \sqrt{\lambda_m^p \lambda_m^u} \; S_m^u H_1^{(2)}(k\bar{S}_m r) e_{zm}^u(z) [e_{xm}^p(z_o)\cos\phi + \alpha_m^p e_{ym}^p(z_o)\sin\phi] \quad , \quad r>r_o \end{aligned} \right\} \tag{39}$$

$$
\begin{aligned}
\pi H_{\phi}^{p} = & -\pi M k^{3} \sum_{m} \Bigg\{ \lambda_{m}^{p} S_{m}^{p} H_{1}^{(2)'}(kS_{m}^{p}r) h_{ym}^{p}(z) \left[e_{xm}^{p}(z_{o}) \cos\phi + \alpha_{m}^{p} e_{ym}^{p}(z_{o}) \sin\phi \right] \\
& + \lambda_{m}^{p} S_{m}^{p} \frac{H_{1}^{(2)}(kS_{m}^{p}r)}{kS_{m}^{p}r} h_{xm}^{p}(z) \left[-e_{xm}^{p}(z_{o}) \sin\phi + \alpha_{m}^{p} e_{ym}^{p}(z_{o}) \cos\phi \right] \Bigg\} \\
& -jk^{2} \sum_{m} \Bigg\{ S_{m}^{p} J_{1}'(kS_{m}^{p}r) h_{ym}^{p}(z) \left[x_{1m} \cos\phi + x_{2m} \sin\phi \right] \\
& + S_{m}^{p} \frac{J_{1}(kS_{m}^{p}r)}{kS_{m}^{p}r} h_{xm}^{p}(z) \left[-x_{1m} \sin\phi + x_{2m} \cos\phi \right] \Bigg\} \qquad , \quad r<r_{o} \\
& = -jk^{2} \sum_{m} \Bigg\{ S_{m}^{u} H_{1}^{(2)'}(kS_{m}^{u}r) h_{ym}^{u}(z) \left[x_{3m} \cos\phi + x_{4m} \sin\phi \right] \\
& + S_{m}^{u} \frac{H_{1}^{(2)}(kS_{m}^{u}r)}{kS_{m}^{u}r} h_{xm}^{u}(z) \left[-x_{3m} \sin\phi + x_{4m} \cos\phi \right] \Bigg\} \qquad , \quad r>r_{o}
\end{aligned}
\tag{34}
$$

$$
\begin{aligned}
\pi H_{r}^{p} = & -\pi M k^{3} \sum_{m} \Bigg\{ \lambda_{m}^{p} S_{m}^{p} H_{1}^{(2)'}(kS_{m}^{p}r) h_{xm}^{p}(z) \left[e_{xm}^{p}(z_{o}) \cos\phi + \alpha_{m}^{p} e_{ym}^{p}(z_{o}) \sin\phi \right] \\
& - \lambda_{m}^{p} S_{m}^{p} \frac{H_{1}^{(2)}(kS_{m}^{p}r)}{kS_{m}^{p}r} h_{ym}^{p}(z) \left[-e_{xm}^{p}(z_{o}) \sin\phi + \alpha_{m}^{p} e_{ym}^{p}(z_{o}) \cos\phi \right] \Bigg\} \\
& -jk^{2} \sum_{m} \Bigg\{ S_{m}^{p} J_{1}'(kS_{m}^{p}r) h_{xm}^{p}(z) \left[x_{1m} \cos\phi + x_{2m} \sin\phi \right] \\
& - S_{m}^{p} \frac{J_{1}(kS_{m}^{p}r)}{kS_{m}^{p}r} h_{ym}^{p}(z) \left[-x_{1m} \sin\phi + x_{2m} \cos\phi \right] \Bigg\} \qquad , \quad r<r_{o} \\
& = -jk^{2} \sum_{m} \Bigg\{ S_{m}^{u} H_{1}^{(2)'}(kS_{m}^{u}r) h_{xm}^{u}(z) \left[x_{3m} \cos\phi + x_{4m} \sin\phi \right] \\
& - S_{m}^{u} \frac{H_{1}^{(2)}(kS_{m}^{u}r)}{kS_{m}^{u}r} h_{ym}^{u}(z) \left[-x_{3m} \sin\phi + x_{4m} \cos\phi \right] \Bigg\} \qquad , \quad r>r_{o}
\end{aligned}
\tag{35}
$$

Since ratios of the perturbed to unperturbed fields are the quantities displayed in the following section, for convenience the unperturbed fields are listed below

$$\sum_m \left(S_m^p Q_{nm}^{up} x_{1m} + jS_m^p \frac{J_1(kS_m^p r_o)}{kS_m^p r_o} R_{nm}^{up} x_{2m} - S_m^u T_{nm}^{uu} x_{3m} - jS_m^u \frac{H_1^{(2)}(kS_m^u r_o)}{kS_m^u r_o} U_{nm}^{uu} x_{4m} \right)$$

$$= j\pi Mk \sum_m \left\{ \lambda_m^p S_m^p \left[e_{xm}^p(z_o) P_{nm}^{up} + j\alpha_m^p e_{ym}^p(z_o) \frac{H_1^{(2)}(kS_m^p r_o)}{kS_m^p r_o} R_{nm}^{up} \right] \right\} \tag{30}$$

$$\sum_m \left[-jS_m^p \frac{J_1(kS_m^p r_o)}{kS_m^p r_o} R_{nm}^{pp} x_{1m} + S_m^p Q_{nm}^{pp} x_{2m} + jS_m^u \frac{H_1^{(2)}(kS_m^u r_o)}{kS_m^u r_o} U_{nm}^{pu} x_{3m} - S_m^u T_{nm}^{pu} x_{4m} \right]$$

$$= j\pi Mk \sum_m \left\{ \lambda_m^p S_m^p \left[\alpha_m^p e_{ym}^p(z_o) P_{nm}^{pp} - je_{xm}^p(z_o) \frac{H_1^{(2)}(kS_m^p r_o)}{kS_m^p r_o} R_{nm}^{pp} \right] \right\} \tag{31}$$

$$\sum_m \left[-jS_m^p \frac{J_1(kS_m^p r_o)}{kS_m^p r_o} R_{nm}^{up} x_{1m} + S_m^p Q_{nm}^{up} x_{2m} + jS_m^u \frac{H_1^{(2)}(kS_m^u r_o)}{kS_m^u r_o} U_{nm}^{uu} x_{3m} - S_m^u T_{nm}^{uu} x_{4m} \right]$$

$$= j\pi Mk \sum_m \left\{ \lambda_m^p S_m^p \left[\alpha_m^p e_{ym}^p(z_o) P_{nm}^{up} - je_{xm}^p(z_o) \frac{H_1^{(2)}(kS_m^p r_o)}{kS_m^p r_o} R_{nm}^{up} \right] \right\} \tag{32}$$

Equations (29) through (32) determine $(x_1, x_2, x_3, x_4)_m$ and in terms of these quantities the field components discussed in the following section are developed from Eqs. (1), (13), (14) and (20) through (23). They are

$$\left.
\begin{aligned}
E_z^p &= j\pi Mk^3 \sum_m \lambda_m^p S_m^p H_1^{(2)}(kS_m^p r) e_{zm}^p(z) \left[e_{xm}^p(z_o)\cos\phi + \alpha_m^p e_{ym}^p(z_o)\sin\phi \right] \\
&\quad -k^2 \sum_m S_m^p J_1(kS_m^p r) e_{zm}^p(z) \left[x_{1m}\cos\phi + x_{2m}\sin\phi \right] \qquad , \qquad r<r_o \\
&= -k^2 \sum_m S_m^u H_1^{(2)}(kS_m^u r) e_{zm}^u(z) \left[x_{3m}\cos\phi + x_{4m}\sin\phi \right] \qquad , \qquad r>r_o
\end{aligned}
\right\} \tag{33}$$

$$
\left.
\begin{aligned}
P_{nm}^{pp} &= \int_{-\infty}^{\infty} [q_n^p(-)]^\dagger P_m dz \quad , \quad Q_{nm}^{pp} = \int_{-\infty}^{\infty} [q_n^p(-)]^\dagger Q_m dz \quad , \quad R_{nm}^{pp} = \int_{-\infty}^{\infty} [q_n^p(-)]^\dagger R_m dz \quad , \\
T_{nm}^{pu} &= \int_{-\infty}^{\infty} [q_n^p(-)]^\dagger T_m dz \quad , \quad U_{nm}^{pu} = \int_{-\infty}^{\infty} [q_n^p(-)]^\dagger U_m dz \quad , \\
P_{nm}^{up} &= \int_{-\infty}^{\infty} [q_n^u(+)]^\dagger P_m dz \quad , \quad Q_{nm}^{up} = \int_{-\infty}^{\infty} [q_n^u(+)]^\dagger Q_m dz \quad , \quad R_{nm}^{up} = \int_{-\infty}^{\infty} [q_n^u(+)]^\dagger R_m dz \quad , \\
T_{nm}^{uu} &= \int_{-\infty}^{\infty} [q_n^u(+)]^\dagger T_m dz \quad , \quad U_{nm}^{uu} = \int_{-\infty}^{\infty} [q_n^u(+)]^\dagger U_m dz
\end{aligned}
\right\} \qquad (28)
$$

In Eq. (28) the dagger sign, †, indicates the adjoint (i.e., the complex conjugate transpose).

To generate the field matching equations, first multiply Eq. (24) through by $\cos\phi$ and integrate ϕ from 0 to 2π. Next multiply through by $[q_n^p(-)]^\dagger$ and integrate over z. If N is the total number of modes used, this generates one equation for the 4 x N unknowns $(x_1, x_2, x_3, x_4)_m$, where m takes on the values 1 through N. Next multiply the equation obtained from the ϕ integration by $(q_n^u(+))^\dagger$ and integrate over z. This generates a second equation. By extracting the $\sin\phi$ terms, two more equations are generated in a similar fashion. Performing these operations for n = 1 through N generates the requisite 4 x N equations. The equations are (here the mode indices are included explicitly):

$$
\sum_m \left[S_m^p Q_{nm}^{pp} x_{1m} + jS_m^p \frac{J_1(kS_m^p r_o)}{kS_m^p r_o} R_{nm}^{pp} x_{2m} - S_m^u T_{nm}^{pu} x_{3m} - jS_m^u \frac{H_1^{(2)}(kS_m^u r_o)}{kS_m^u r_o} U_{nm}^{pu} x_{4m} \right]
$$

$$
= j\pi Mk \sum_m \left\{ \lambda_m^p S_m^p \left[e_{xm}^p(z_o) P_{nm}^{pp} + j\alpha_m^p e_{ym}^p(z_o) \frac{H_1^{(2)}(kS_m^p r_o)}{kS_m^p r_o} R_{nm}^{pp} \right] \right\} \qquad (29)
$$

As discussed by Pappert and Smith [1972], there exists height gains

$$q_m^p(-) = \begin{bmatrix} w_1^p(z) \\ w_2^p(z) \\ w_3^p(z) \\ w_4^p(z) \end{bmatrix}_m \qquad q_m^u(+) = \begin{bmatrix} w_1^u(z) \\ w_2^u(z) \\ w_3^u(z) \\ w_4^u(z) \end{bmatrix}_m \tag{26}$$

associated with an adjoint guide for which the inner products $[q_n^p(-), f_m^p(-)]$ and $[q_n^u(+), f_m^u(+)]$ are zero when $m \neq n$. The matching equations will be developed by a method somewhat akin to the treatment of mode conversion in the VLF band [Pappert and Snyder, 1972], although it is by no means clear in the present case that it is an optimum or preferred procedure. As will be seen later, the method does have the convenient consequence that it is essentially equivalent to simply matching H_ϕ and E_z at $r = r_o$ at the ground. As a preliminary to developing the matching equations, the following definitions will be useful:

$$P_m = \begin{bmatrix} jH_1^{(2)'}(kS^p r_o)e_y^p(z) \\ H_1^{(2)}(kS^p r_o)e_z^p(z) \\ jH_1^{(2)'}(kS^p r_o)h_y^p(z) \\ H_1^{(2)}(kS^p r_o)h_z^p(z) \end{bmatrix}_m, \quad Q_m = \begin{bmatrix} jJ_1'(kS^p r_o)e_y^p(z) \\ J_1(kS^p r_o)e_z^p(z) \\ jJ_1'(kS^p r_o)h_y^p(z) \\ J_1(kS^p r_o)h_z^p(z) \end{bmatrix}_m, \quad R_m = \begin{bmatrix} e_x^p(z) \\ 0 \\ h_x^p(z) \\ 0 \end{bmatrix}_m$$

$$T_m = \begin{bmatrix} jH_1^{(2)'}(kS^u r_o)e_y^u(z) \\ H_1^{(2)}(kS^u r_o)e_z^u(z) \\ jH_1^{(2)'}(kS^u r_o)h_y^u(z) \\ H_1^{(2)}(kS^u r_o)h_z^u(z) \end{bmatrix}_m, \quad U_m = \begin{bmatrix} e_x^u(z) \\ 0 \\ h_x^u(z) \\ 0 \end{bmatrix}_m \tag{27}$$

$$+jS^p \frac{J_1(kS^p r_o)}{kS^p r_o}(-x_1\sin\phi + x_2\cos\phi)\begin{bmatrix} e_x^p(z) \\ 0 \\ h_x^p(z) \\ 0 \end{bmatrix}\Bigg\}_m$$

$$= -k^2 \sum_m \Bigg\{ S^u (x_3\cos\phi + x_4\sin\phi) \begin{bmatrix} jH_1^{(2)'}(kS^u r_o) e_y^u(z) \\ H_1^{(2)}(kS^u r_o) e_z^u(z) \\ jH_1^{(2)'}(kS^u r_o) h_y^u(z) \\ H_1^{(2)}(kS^u r_o) h_z^u(z) \end{bmatrix}$$

$$+ jS^u \frac{H_1^{(2)}(kS^u r_o)}{kS^u r_o}(-x_3\sin\phi + x_4\cos\phi)\begin{bmatrix} e_x^u(z) \\ 0 \\ h_x^u(z) \\ 0 \end{bmatrix}\Bigg\}_m \qquad (24)$$

In Eq. (24) the top element of the column vector is E_ϕ, the second E_z, the third ηH_ϕ, and the last is ηH_z. The left-hand side of the equation gives the fields associated with the perturbed region at $r = r_o$ and the right-hand side gives the fields associated with the unperturbed region at $r = r_o$.

With a finite number of modes (and in the present case only one non-evanescent mode exists) it is impossible to satisfy Eq. (24) for all z. Thus, the continuity will be developed only approximately following a prescription suggested by asymptotic considerations when $|kS^p r_o| >> 1$ and $|kS^u r_o| >> 1$. In that instance the leading terms of the forward (+) and backward (-) propagating waves associated with Eq. (24) becomes a product of radial functions and the column vectors

$$f_m^p(\pm) = \begin{bmatrix} \pm e_y^p(z) \\ e_z^p(z) \\ \pm h_y^p(z) \\ h_z^p(z) \end{bmatrix}_m \quad , \quad f_m^u(+) = \begin{bmatrix} e_y^u(z) \\ e_z^u(z) \\ h_y^u(z) \\ h_z^u(z) \end{bmatrix}_m \qquad (25)$$

A disquieting feature of the analysis is that the TE components, and in particular the H_r component, are not continuous at $r = r_o$. This is not terribly surprising because, as just mentioned, the method used to obtain the boundary equations is equivalent to matching only the H_ϕ and E_z components at $r = r_o$ at the ground. Perhaps inclusion of evanescent modes would improve continuity of H_r without destroying the H_ϕ and E_z continuity. However, no effort along those lines has been attempted in the current study.

Several possible extensions of the present effort are:

i) Examine effects of non-evanescent modes on continuity of major field components.

ii) Extend analysis to allow for general location of the disturbance relative to the transmitter.

iii) Extend analysis to allow for radial and/or azimuthal variations.

iv) Include the effect of earth curvature.

v) Extend the analysis to elliptically symmetric disturbances.

REFERENCES

Bickel, J.E., J.A. Ferguson, and G.V. Stanley, "Experimental observation of magnetic field effects on VLF propagation at night," Radio Sci., 5(1), 19-25, 1970.

Budden, K.G., Radio waves in the Ionosphere, (Cambridge Univ. Press, Cambridge), 1961.

Budden, K.G., "The influence of the earth's magnetic field on radio propagation by waveguide modes," Proc. Roy. Soc. (London), Ser. A265 (1323), 538-553, 1962.

Ferguson, J.A., L.R. Hitney and R.A. Pappert, A Program to Compute Vertical Electric ELF Fields in a Laterally Inhomogeneous Earth Ionosphere Waveguide, NOSC TR 851, prepared for the Def. Nucl. Agency, 62 pp, Dec 1982.

Field, E.C. and R.G. Joiner, "An integral equation approach to long wave propagation in a non stratified earth ionosphere waveguide," Radio Sci., 14(6), 1057-1068, 1979.

Field, E.C. and R.G. Joiner, "Effects of lateral ionospheric gradients on ELF propagation," Radio Sci., 17(3), 693-700, 1982.

Greifinger, C. and P. Greifinger, Effects of a Cylindrically Symmetric Ionospheric Disturbance on ELF Propagation in the Earth Ionosphere Waveguide, Def. Nucl. Agency Rep. DNA 4399T, 40 pp., R & D Associates, Marina del Rey, Calif., June 1977.

Pappert, R.A., On the Problem of Horizontal Dipole Excitation of the Earth-Ionosphere Waveguide. Interim report No. 724 prepared by the Naval Electronics Laboratory Center (now NOSC) for the Defense Atomic Support Agency (now DNA), March 1968.

Pappert, R.A. and R.R. Smith, "Orthogonality of VLF height gains in the earth ionosphere waveguide," Radio Sci., 7(2), 275-278, 1972.

Pappert, R.A. and F.P. Snyder, "Some results of a mode conversion program for VLF," Radio Sci., 7(10), 913-923, 1972.

Pappert, R.A. and W.F. Moler, "A theoretical study of ELF normal mode reflection and absorption produced by nighttime ionospheres," J. Atmos. Terr. Phys., 40(9), 1031-1045, 1978.

Pappert, R.A., "Effects of a large patch of sporadic-E on nighttime propagation at lower ELF," J. Atmos. Terr. Phys., 42(5), 417-425, 1980.

Pappert, R.A., "Calculated effects of traveling sporadic-E on nocturnal ELF propagation. Comparison with measurement," Radio Sci., 20(2), 229-246, 1985.

Pitteway, M.L.V., "The numerical calculation of wave-fields, reflection coefficients and polarizations for long radio waves in the lower ionosphere." I, Phil. Trans. Roy. Soc. (London), Ser. A257 (1079), 219-241, 1965.

Shellman, C.H., Propagation of ELF Waves in the Spherical Earth-Ionosphere Waveguide with Transverse and Longitudinal Variation of Properties, NOSC TD 607, prepared for the Def. Nucl. Agency, 194 pp., June 1983.

Smith, R.R., A Program to Compute Ionospheric Height Gain Functions and Field Strengths. Interim Report No. 711 prepared by the Naval Electronics Laboratory Center (now NOSC) for the Defense Atomic Support Agency (now DNA), December 1970.

Wait, J.R., "The mode theory of VLF radio propagation for a spherical earth and a concentric anisotropic ionosphere," Can. J. Phys., 41(2), 299-315, 1963.

Wait, J.R., "On phase changes in very-low frequency propagation induced by an ionospheric depression of finite extent," J. Geophys. Res., 59(3), 441-445, 1964.

Webber, G.E. and I.C. Peden, "VLF fields of a horizontal dipole below the polar anisotropic ionosphere," IEEE Transactions on Antennas and Propagation, AP-19(4), 523-529, 1971.

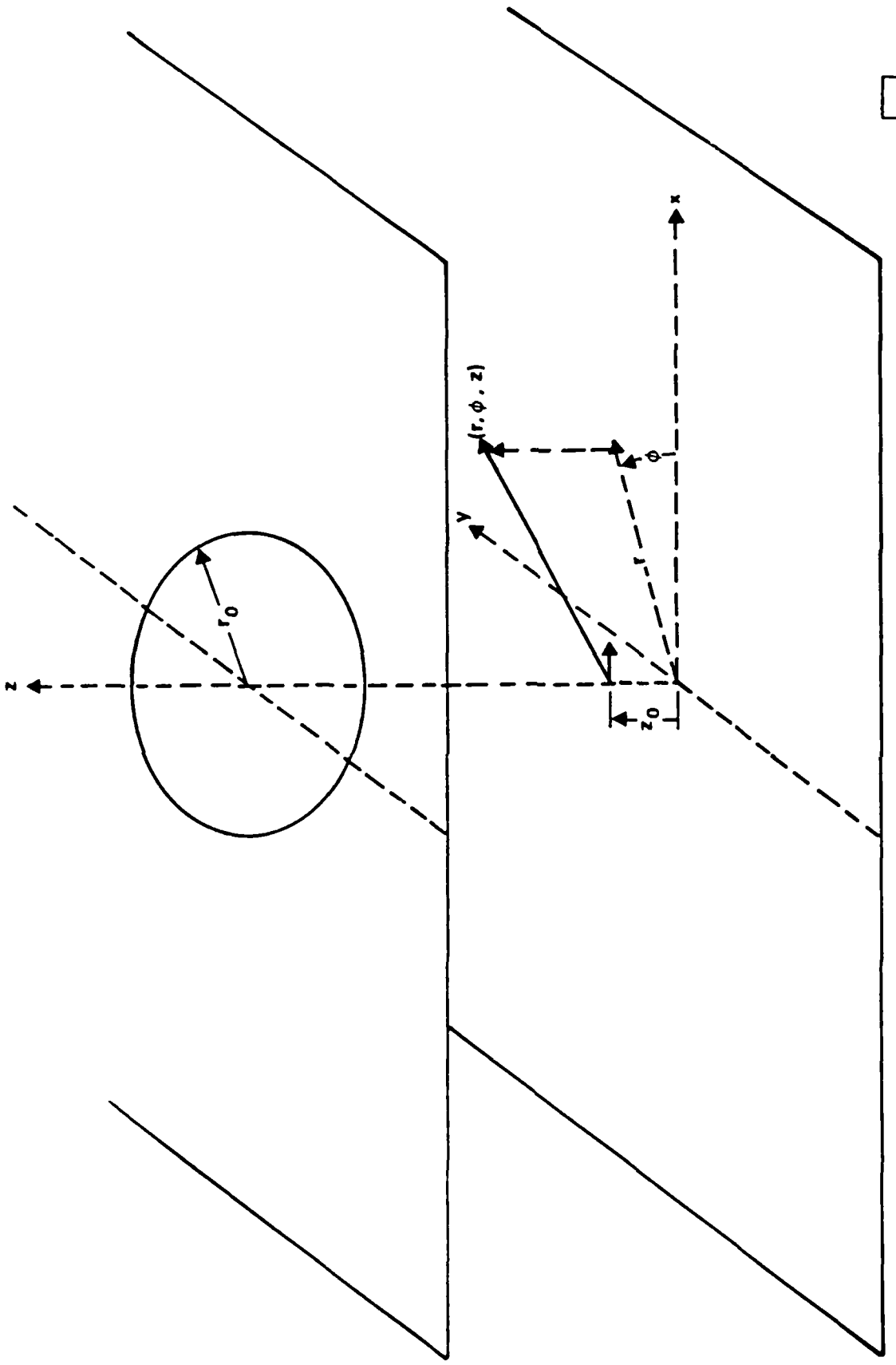

Figure 1. Source and waveguide geometry.

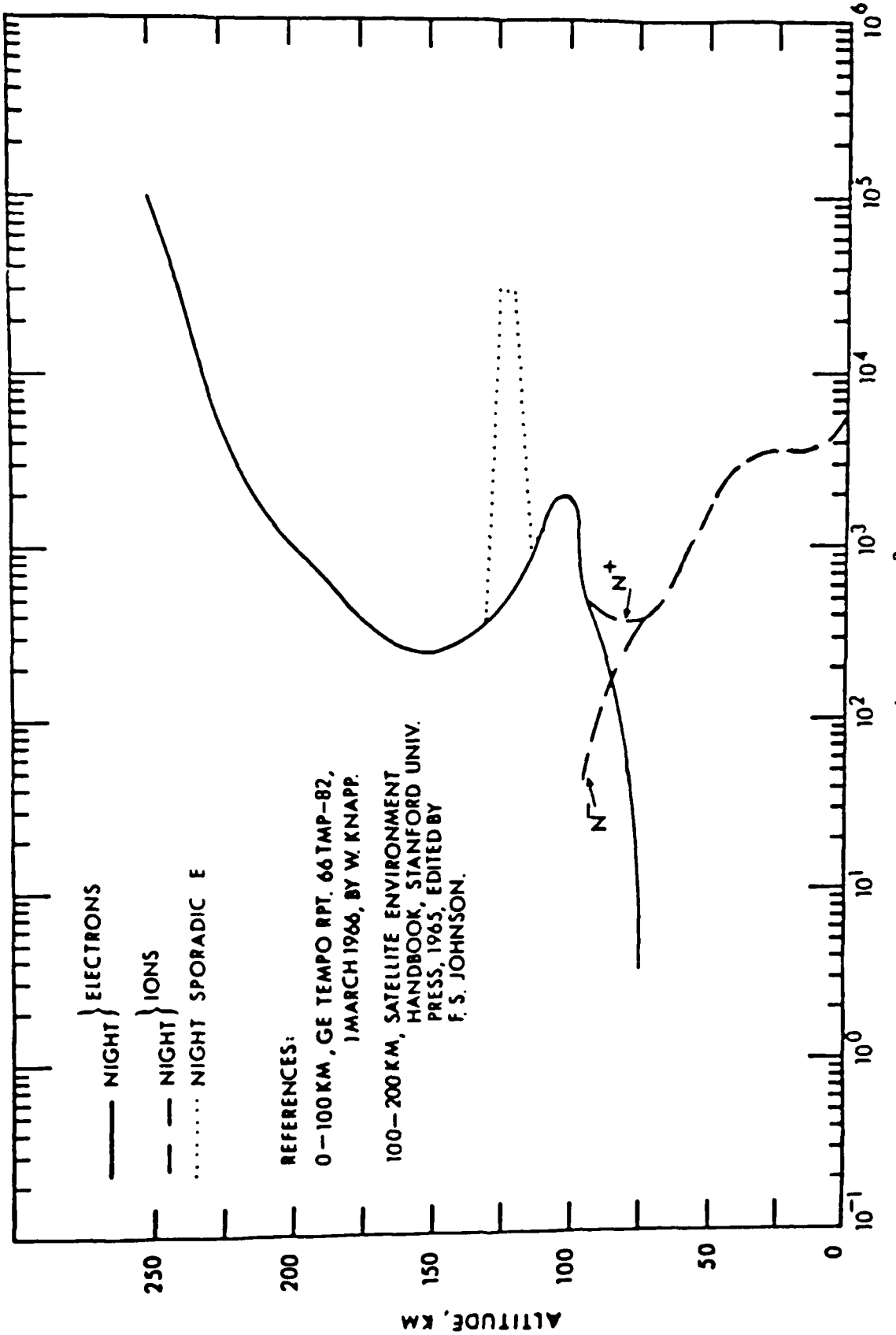

Figure 2. Night ambient and sporadic E profiles.

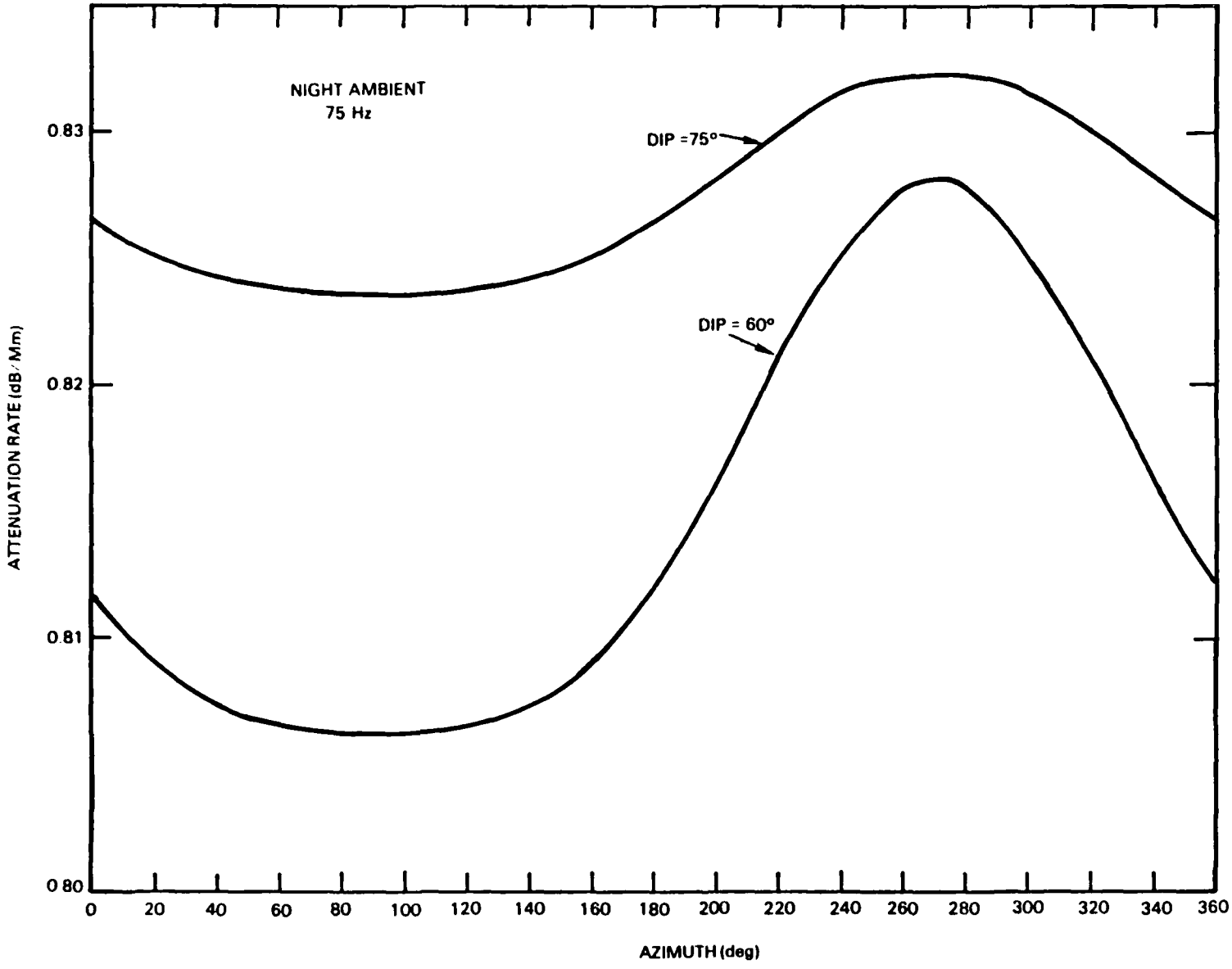

Figure 3. Azimuthal variation of attenuation rate for night ambient profile.

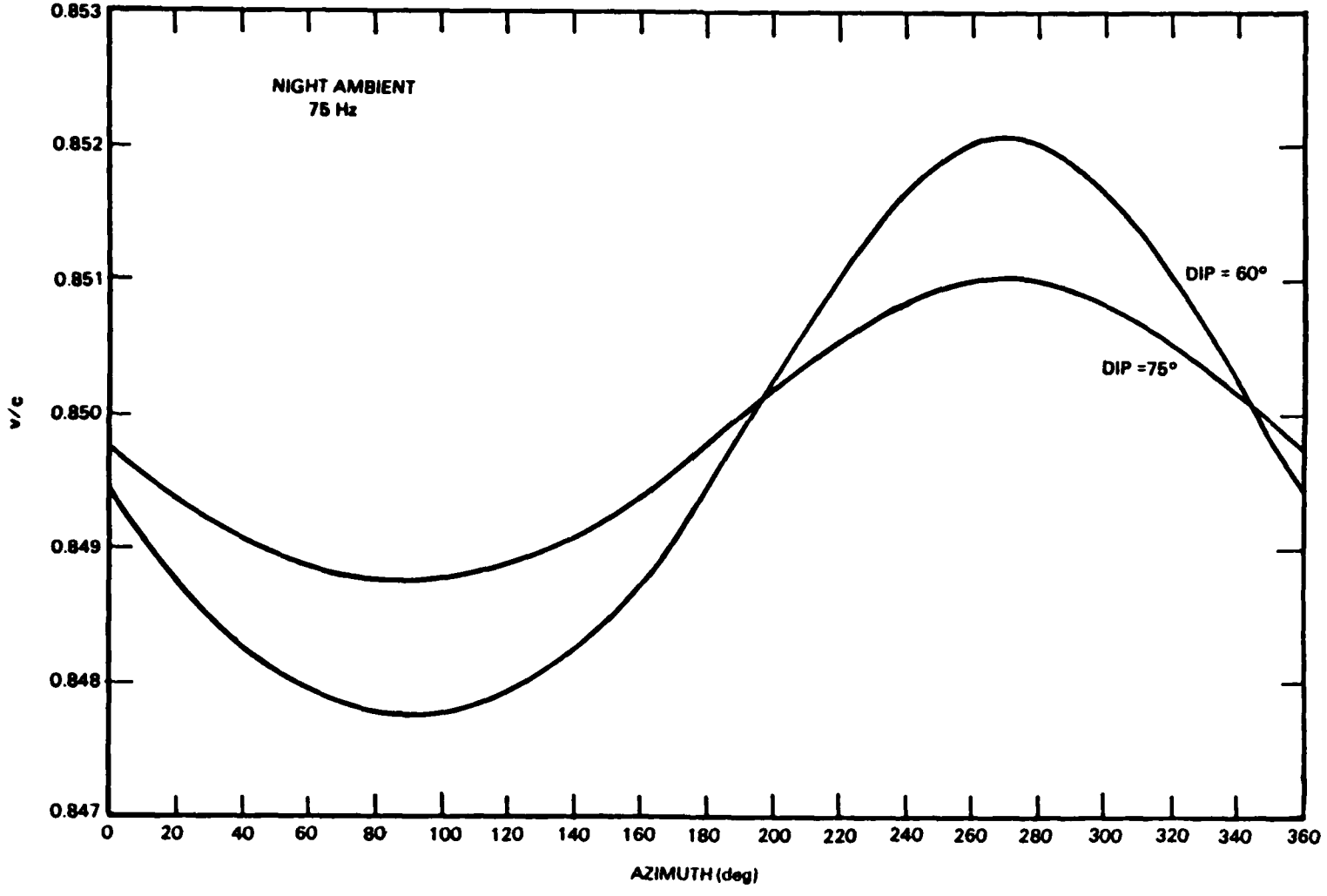

Figure 4. Azimuthal variation of normalized phase velocity for night ambient profile.

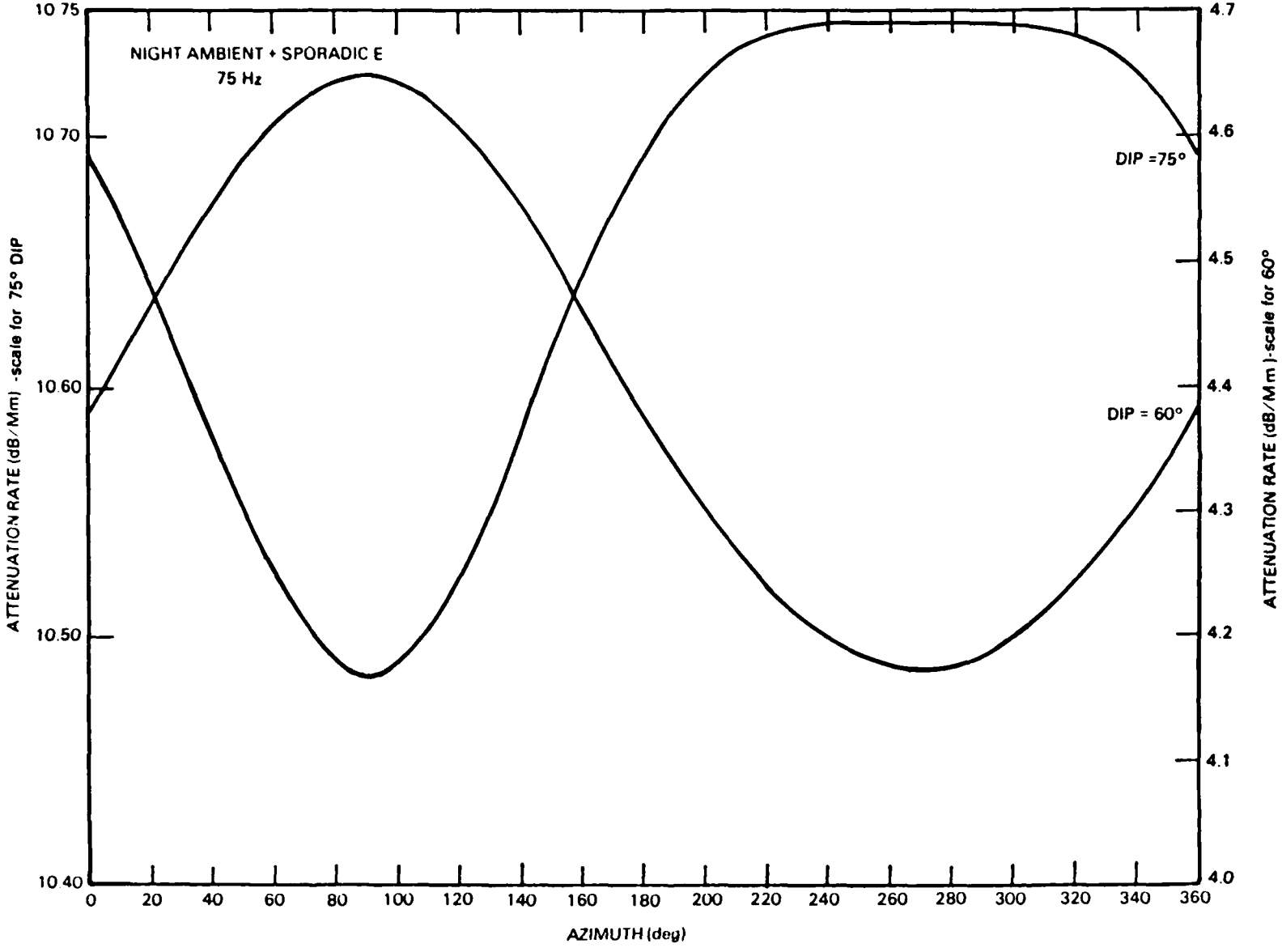

Figure 5. Azimuthal variation of attenuation rate for night ambient profile plus sporadic E.

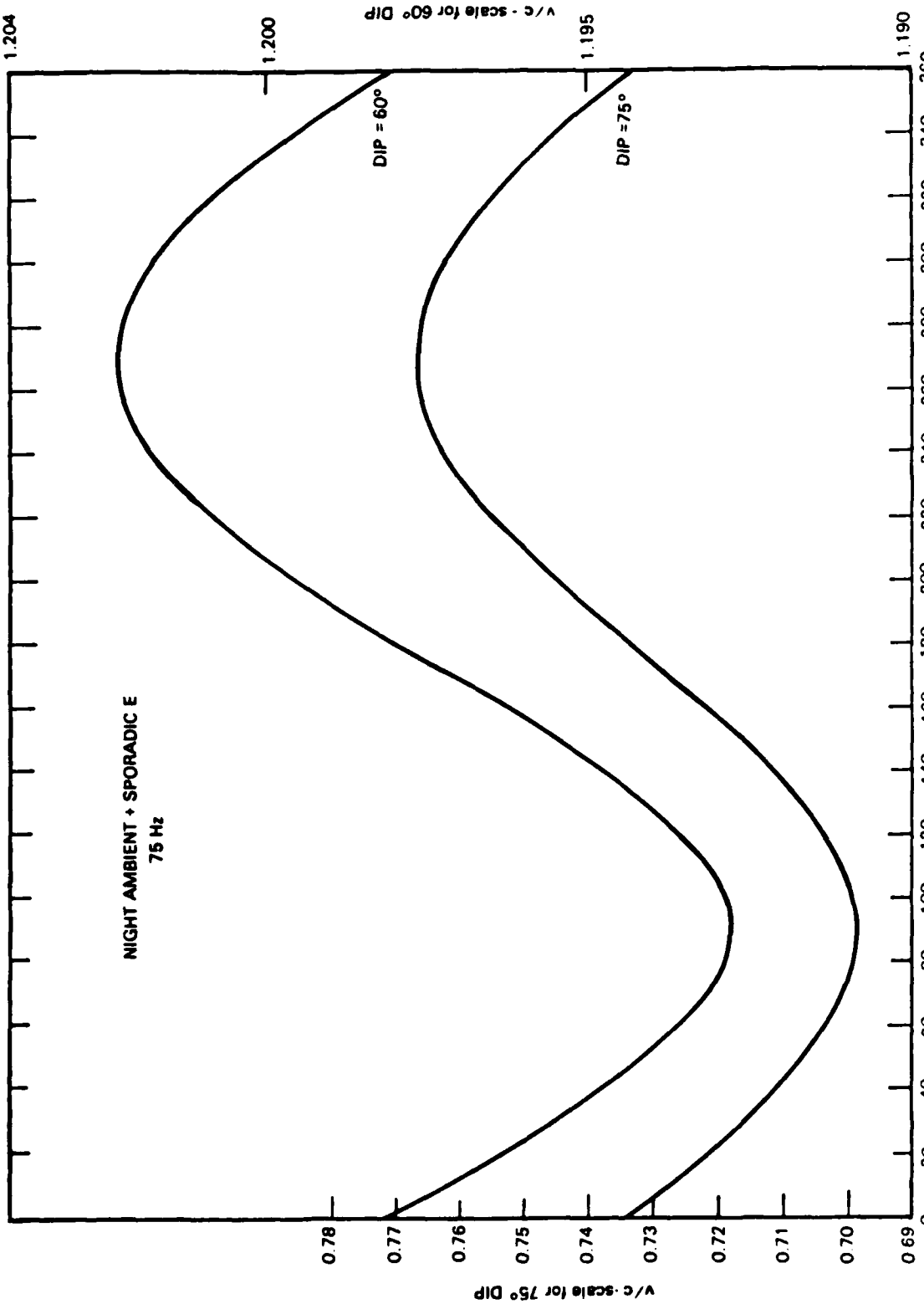

Figure 6. Azimuthal variation of normalized phase velocity for night ambient profile plus sporadic E.

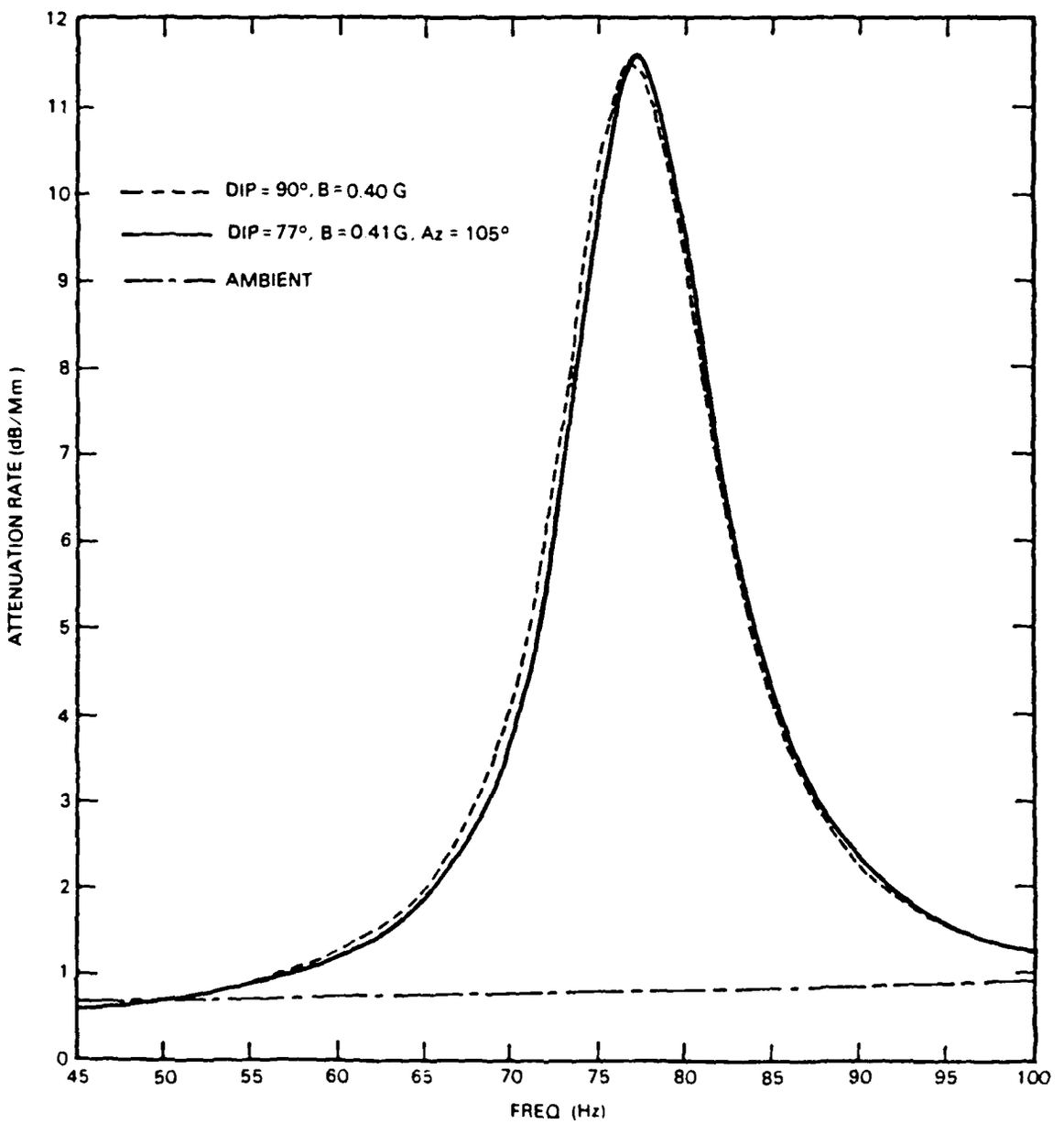

Figure 7. Attenuation rate vs. frequency.

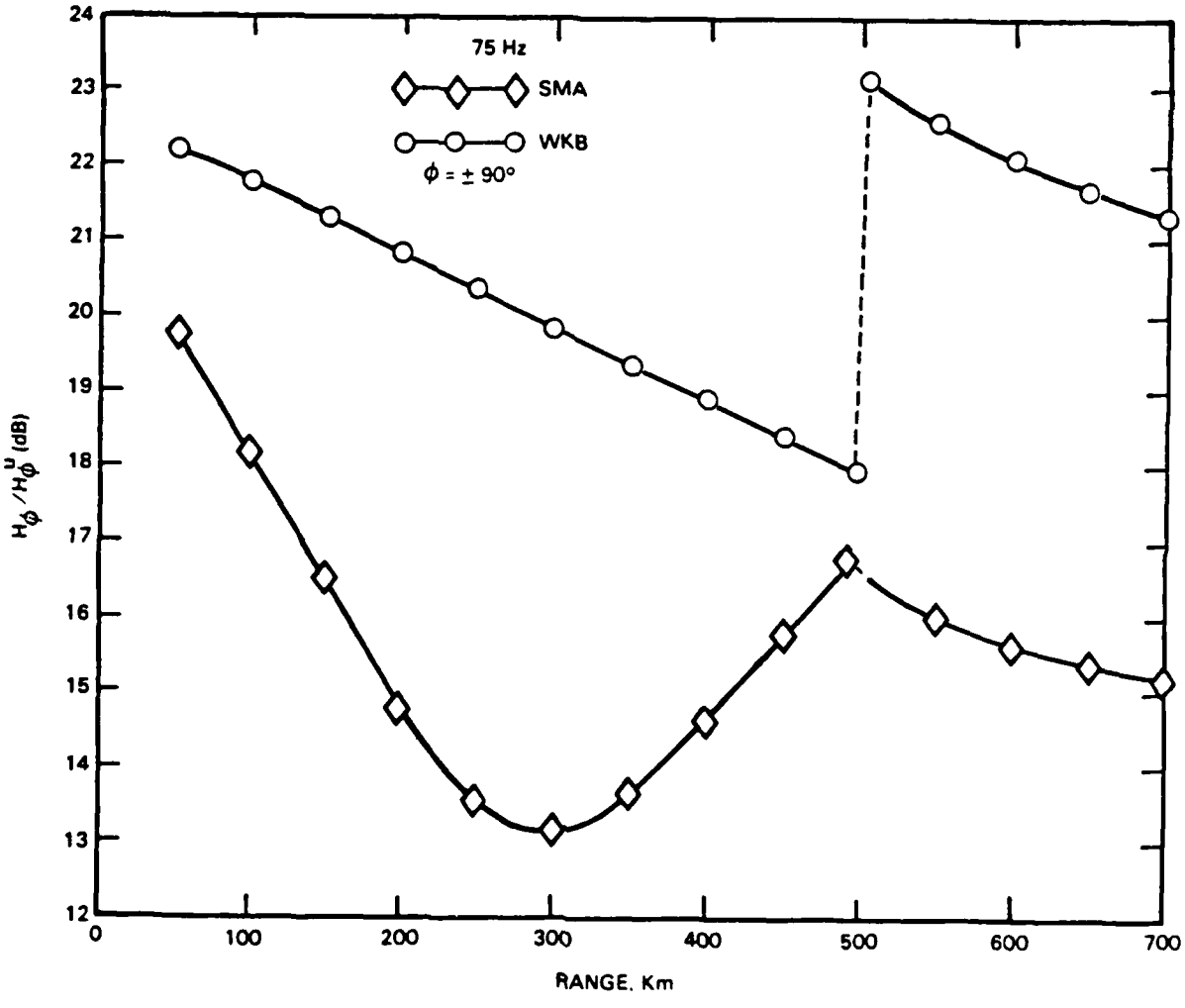

Figure 8. Ratio of disturbed to undisturbed H_ϕ in dB vs. range.

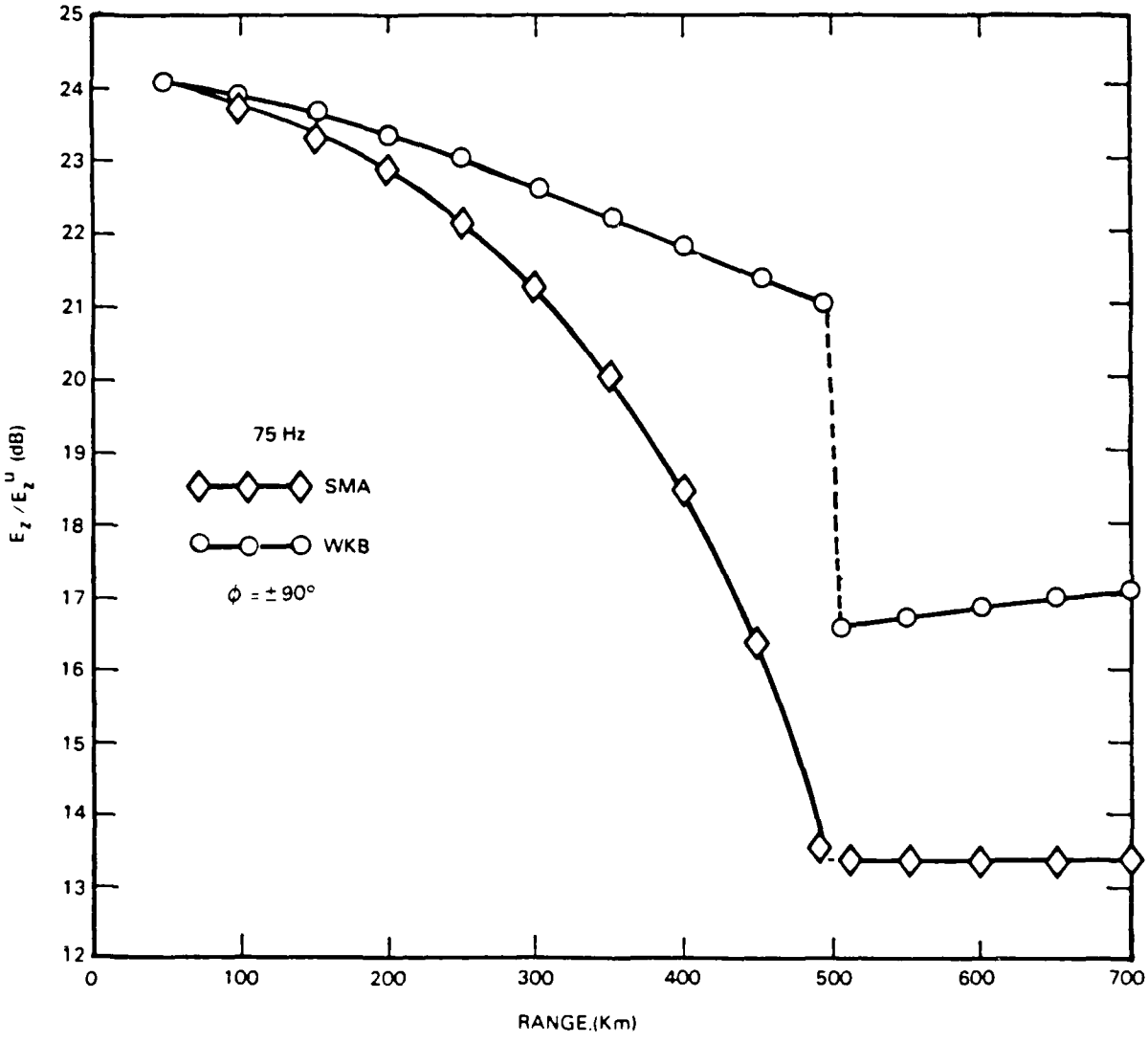

Figure 9. Ratio of disturbed to undisturbed E_z in dB vs. range.

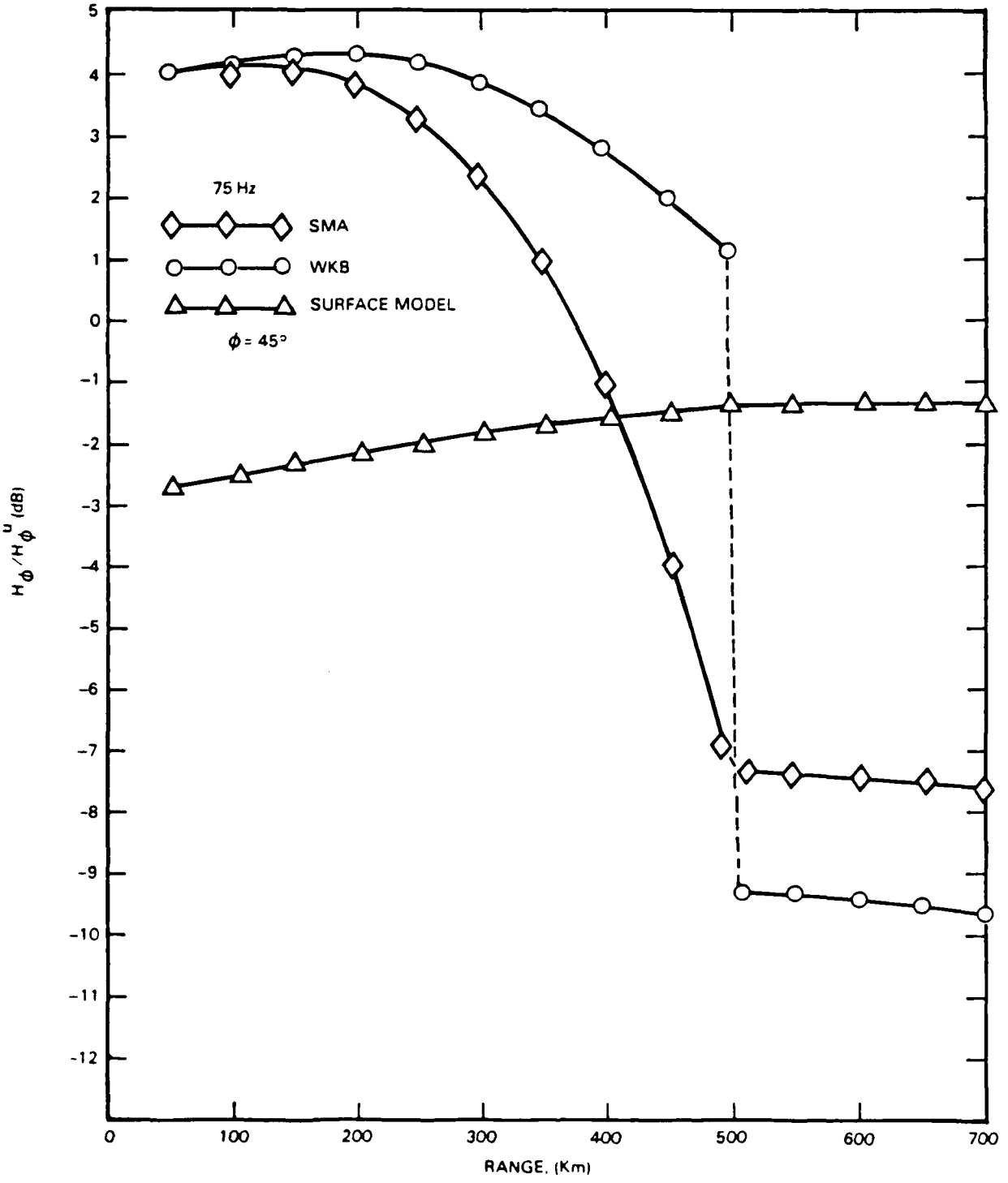

Figure 10. Ratio of disturbed to undisturbed H_ϕ in dB vs. range.

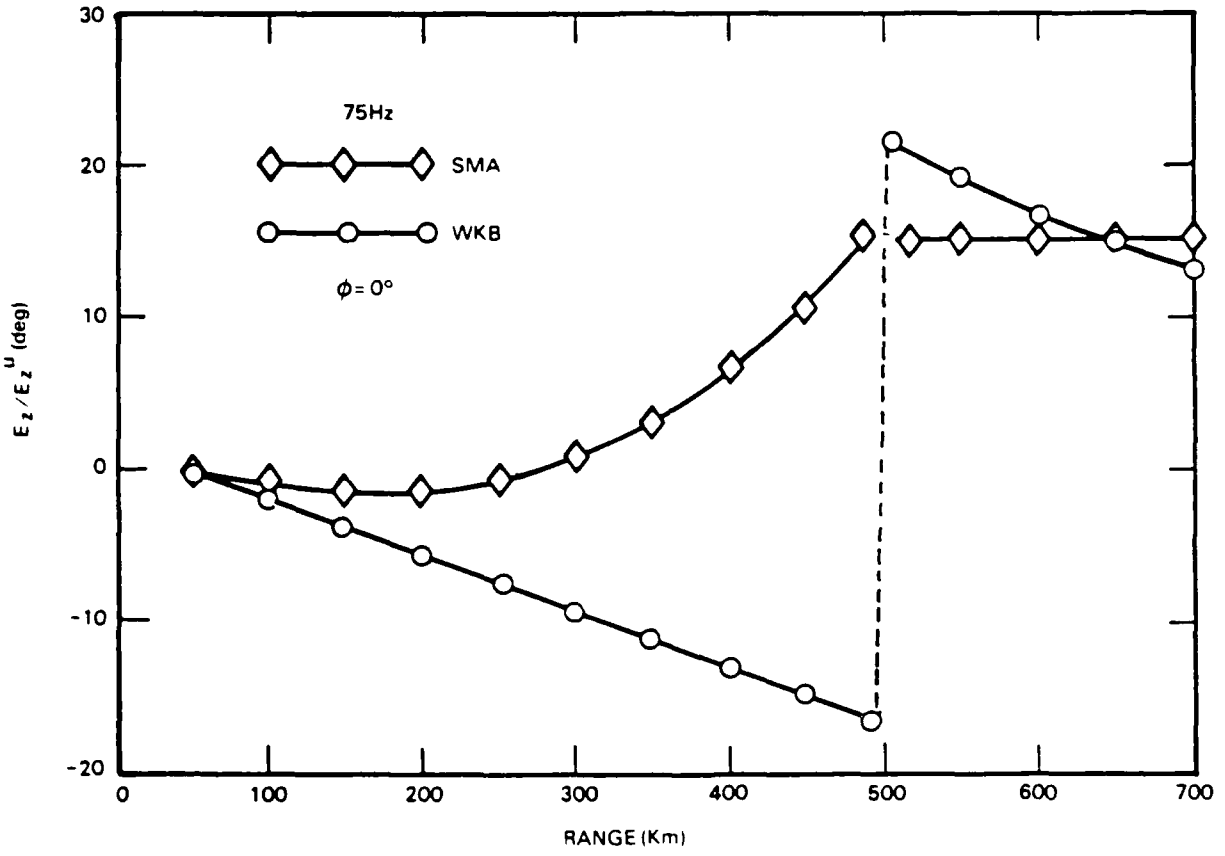

Figure 24. Disturbed and undisturbed phase difference for E_z vs. range.

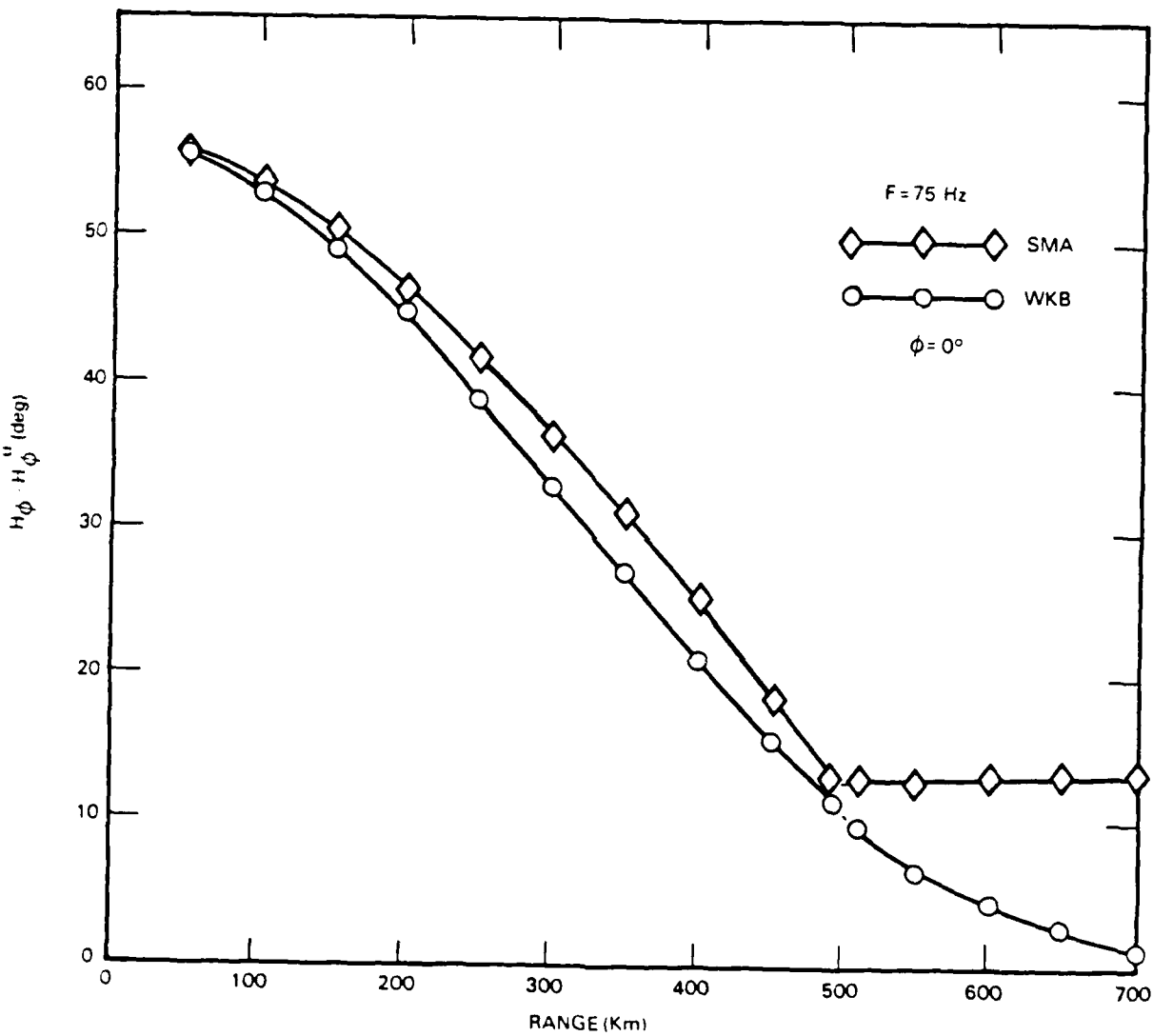

Figure 23. Disturbed and undisturbed phase difference for H_ϕ vs. range.

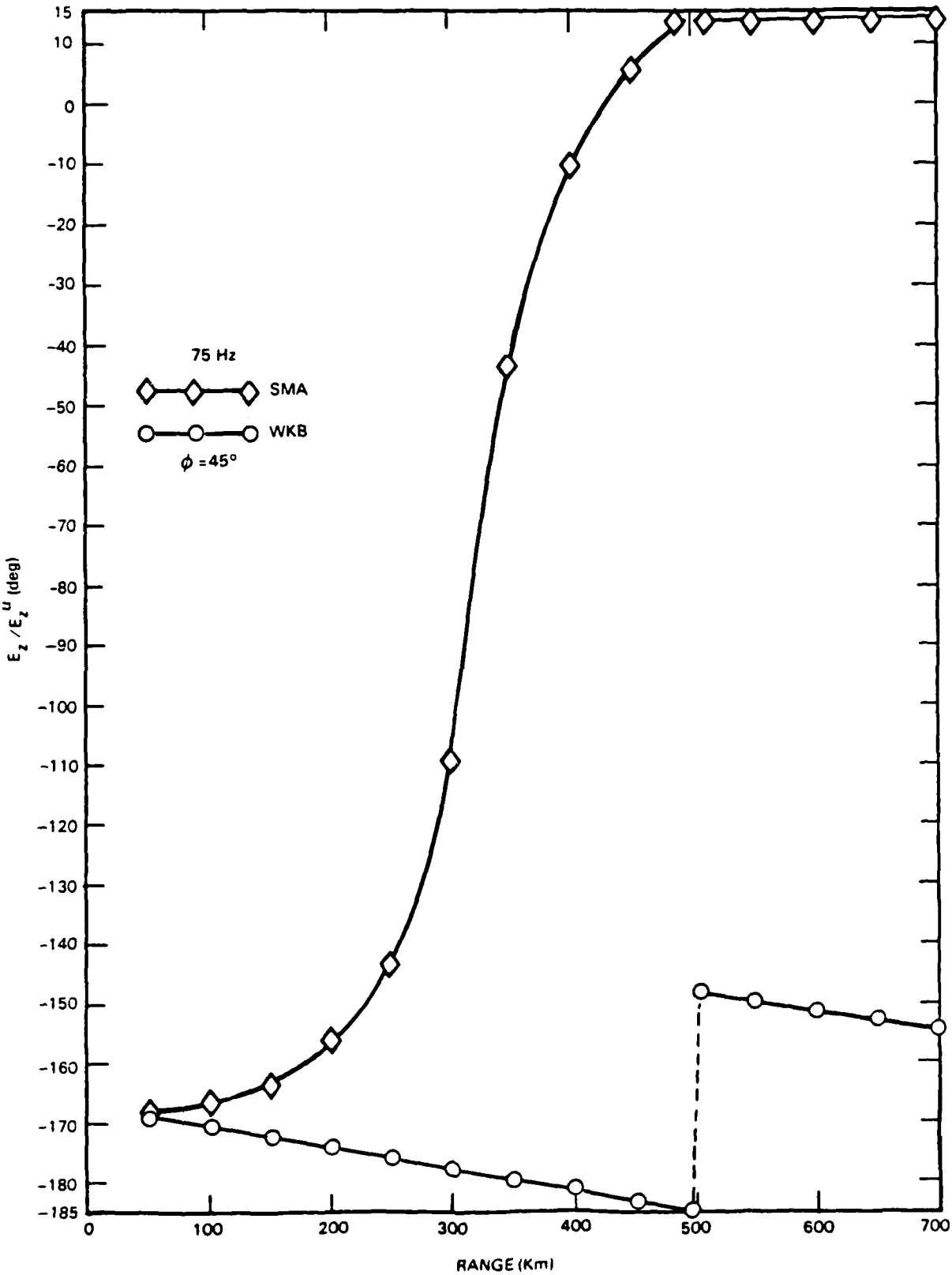

Figure 22. Disturbed and undisturbed phase difference for E_z vs. range.

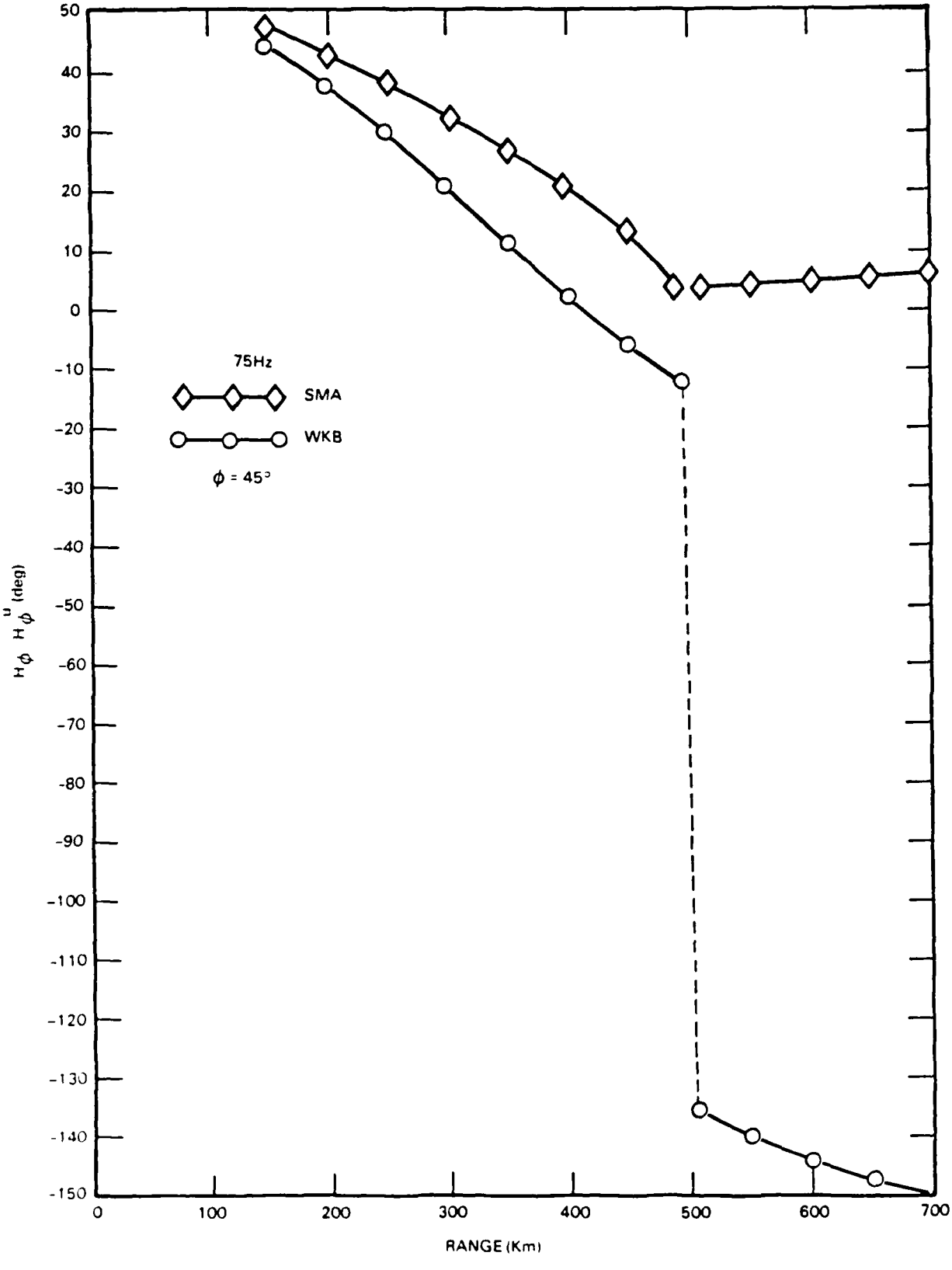

Figure 21. Disturbed and undisturbed phase difference for H_ϕ vs. range.

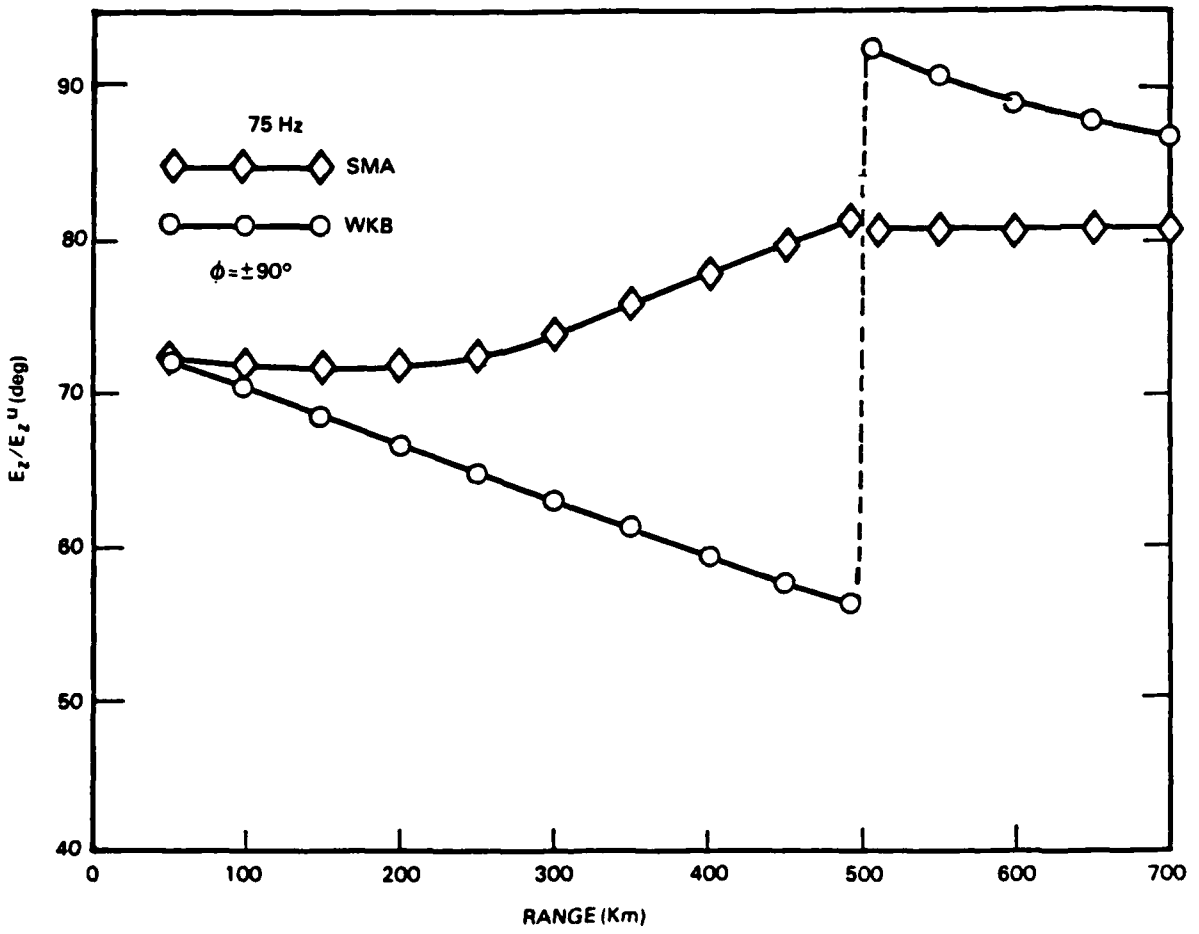

Figure 20. Disturbed and undisturbed phase difference for E_z vs. range.

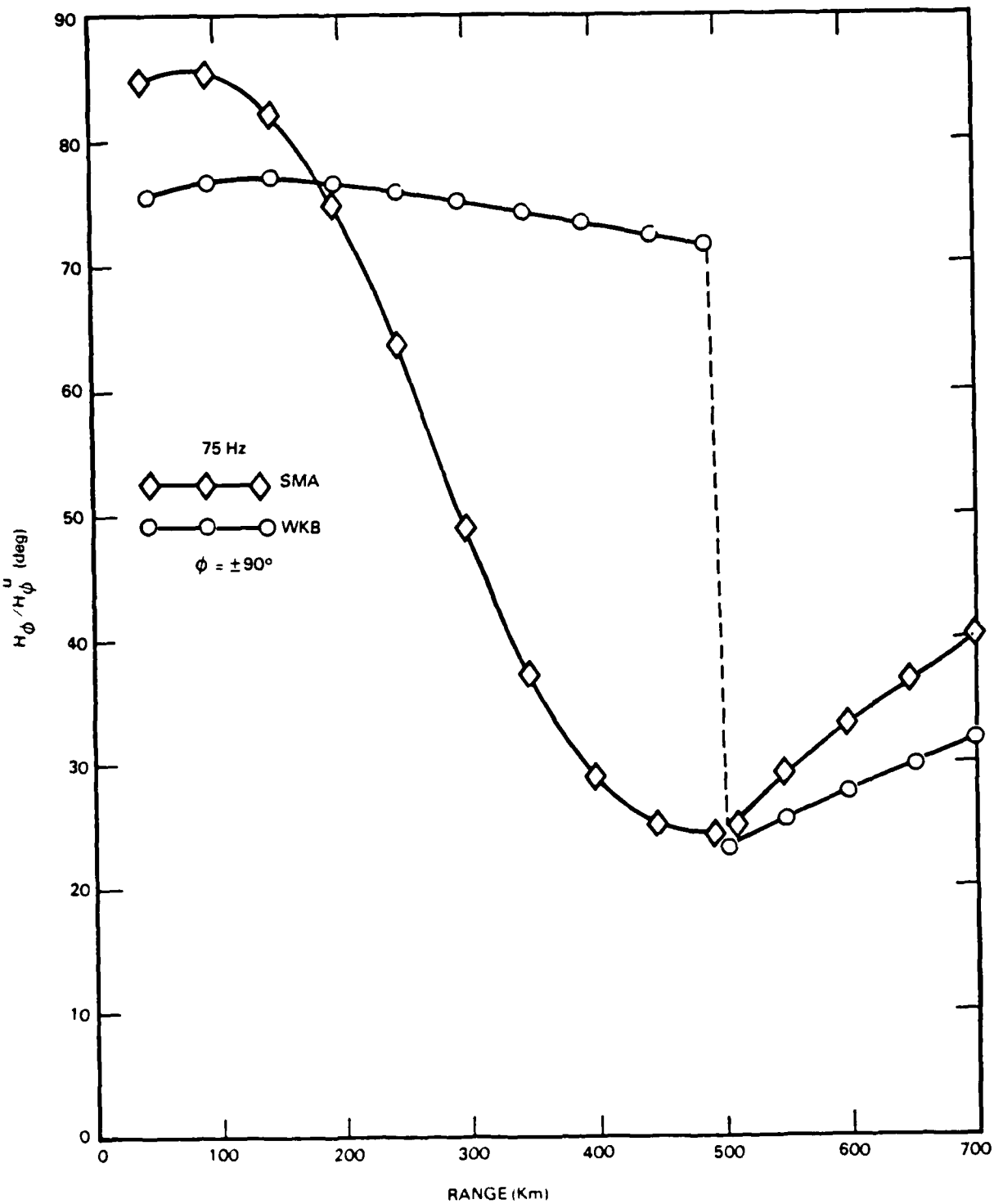

Figure 19. Disturbed and undisturbed phase difference for H_ϕ vs. range.

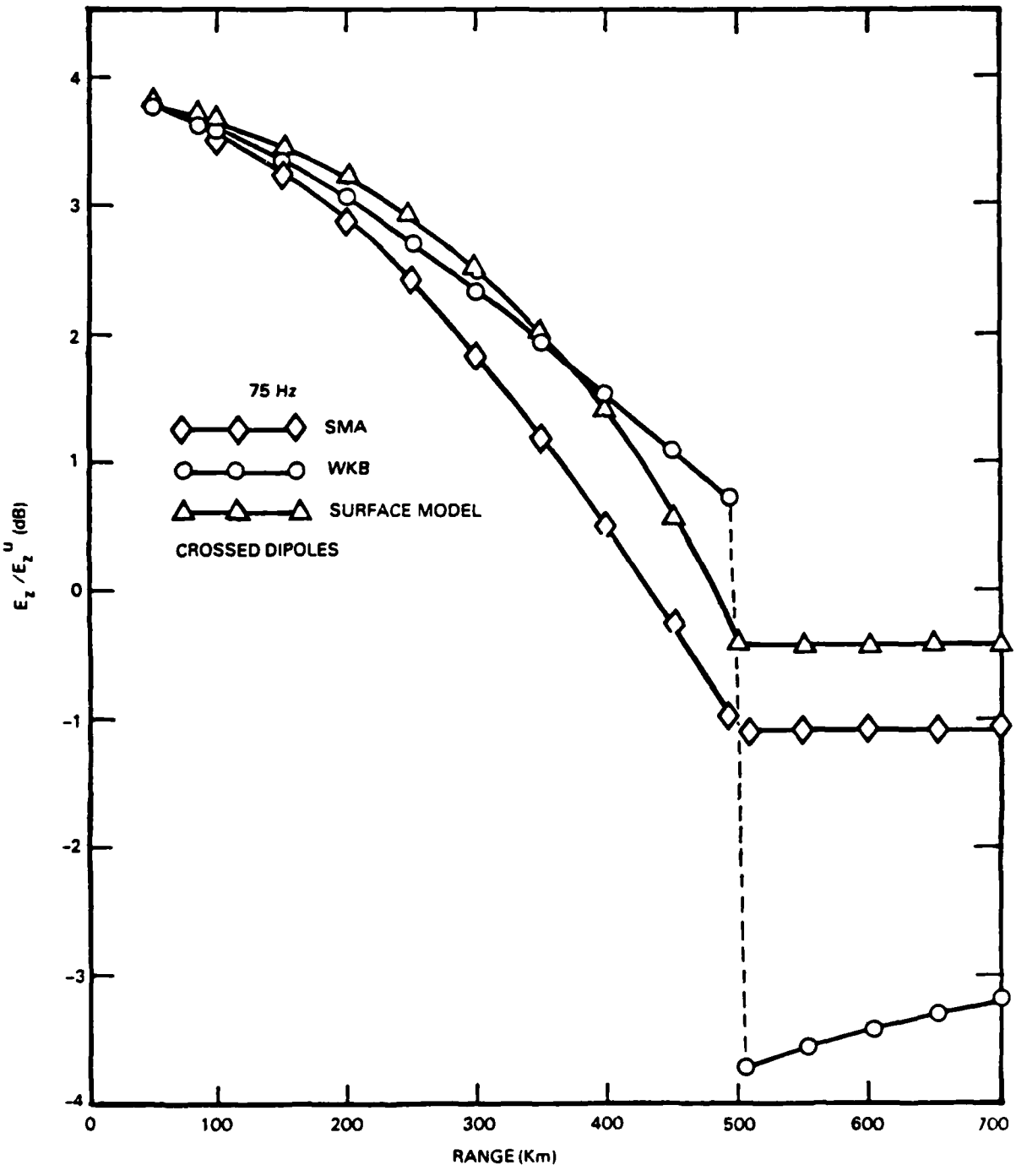

Figure 18. Ratio of disturbed to undisturbed E_z in dB vs. range.

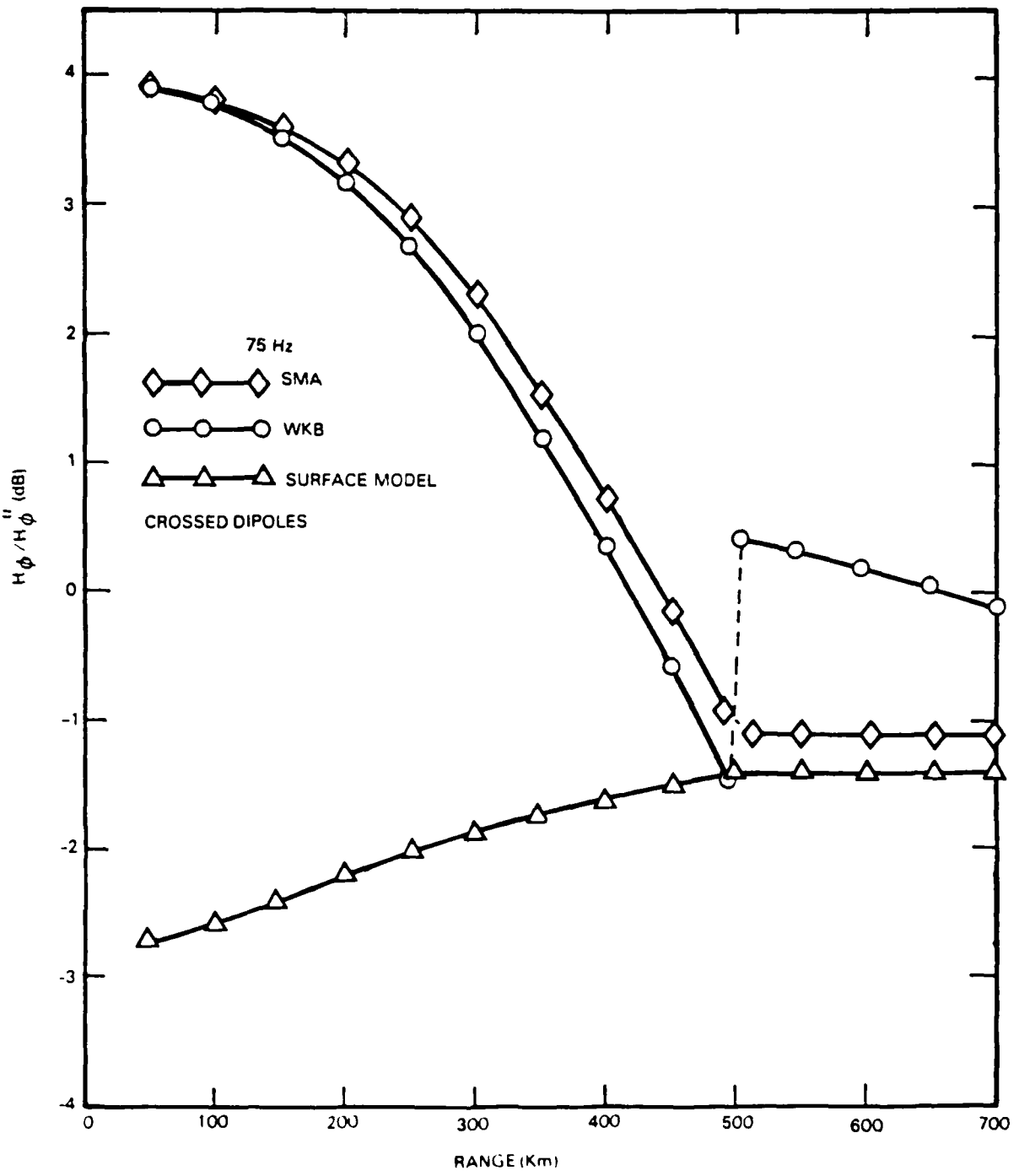

Figure 17. Ratio of disturbed to undisturbed H_ϕ in dB vs. range.

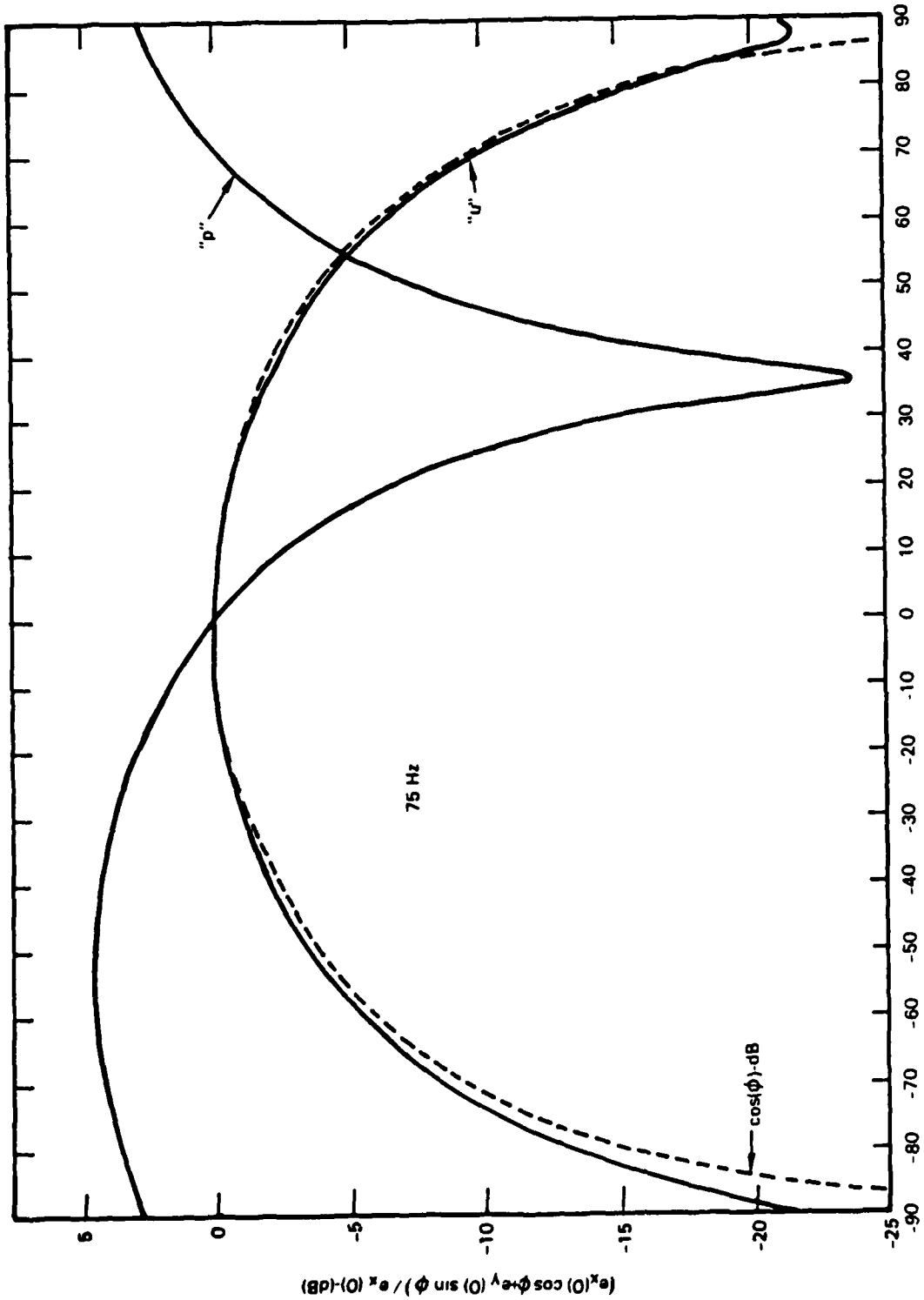

Figure 16. Excitation efficiency of height gains vs. azimuth.

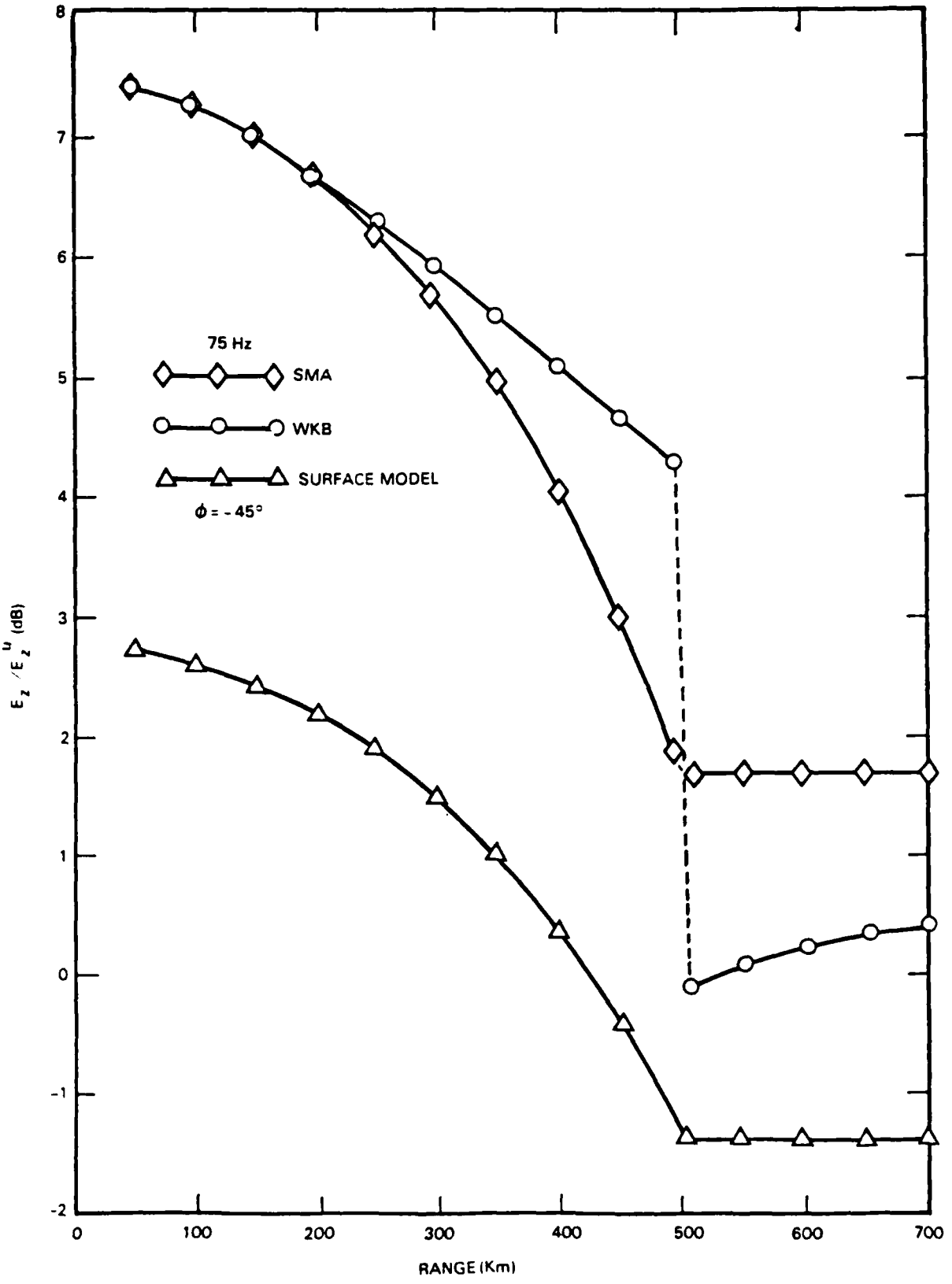

Figure 15. Ratio of disturbed to undisturbed E_z in dB vs. range.

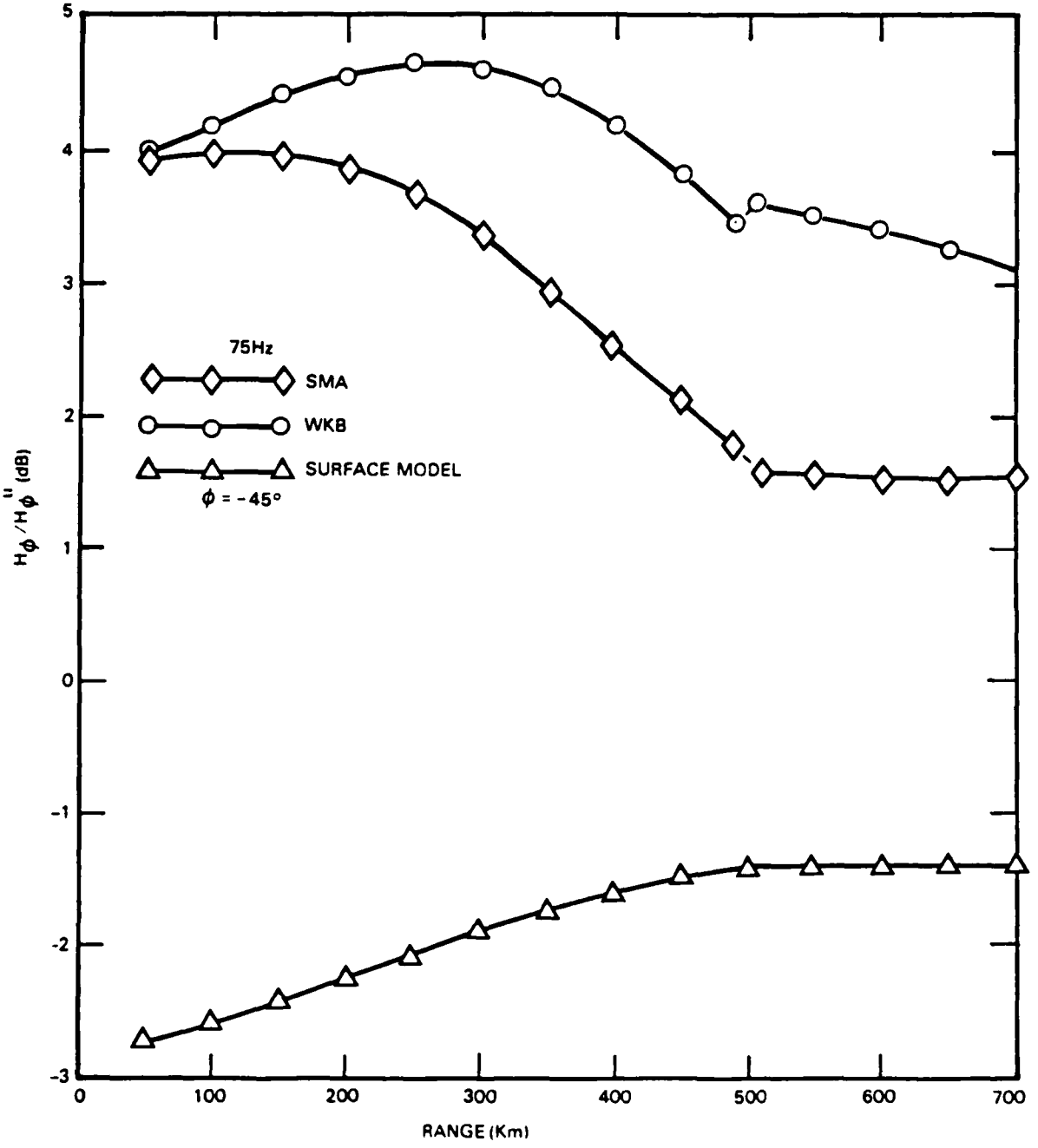

Figure 14. Ratio of disturbed to undisturbed H_ϕ in dB vs. range.

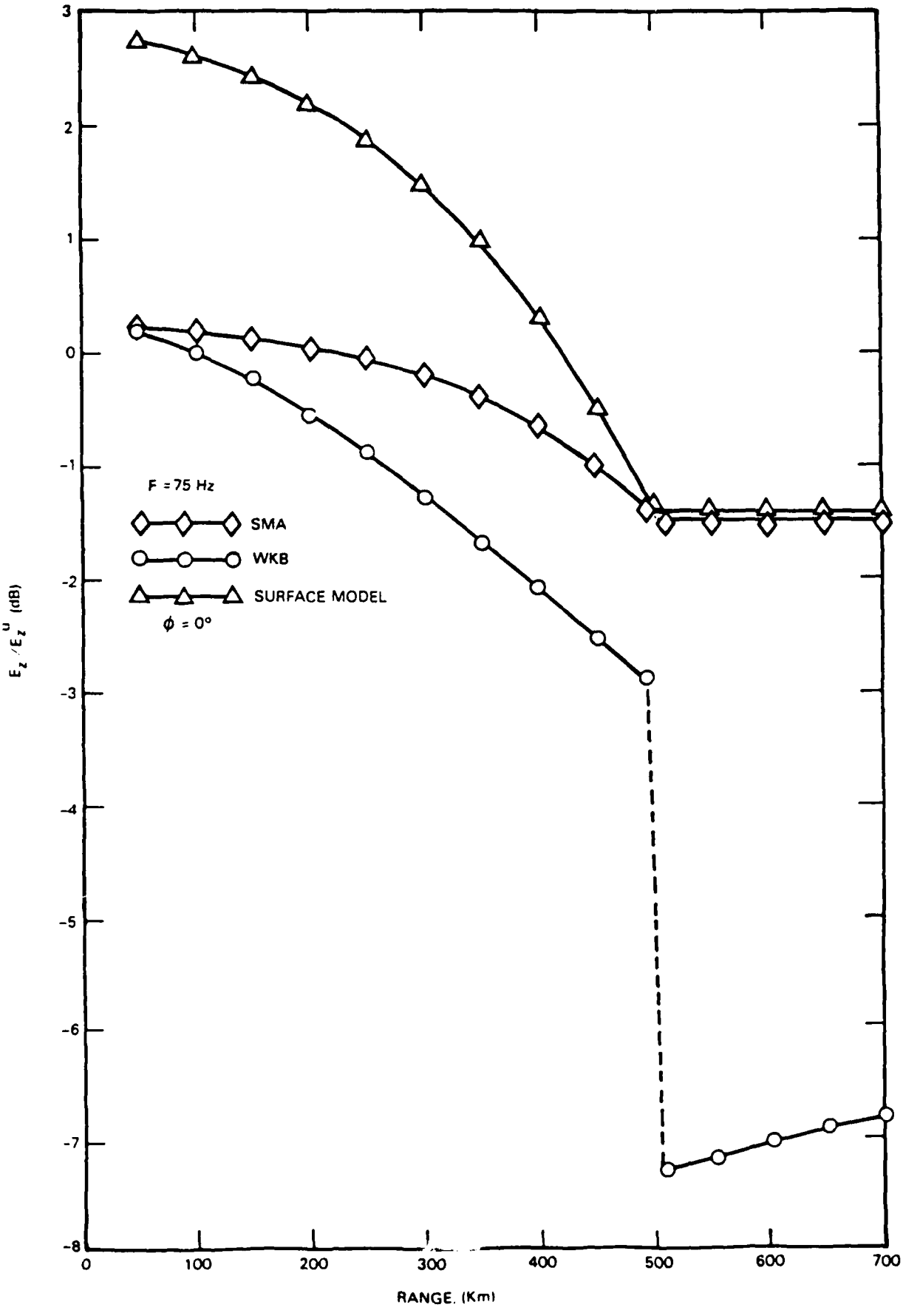

Figure 13. Ratio of disturbed to undisturbed E_z in dB vs. range.

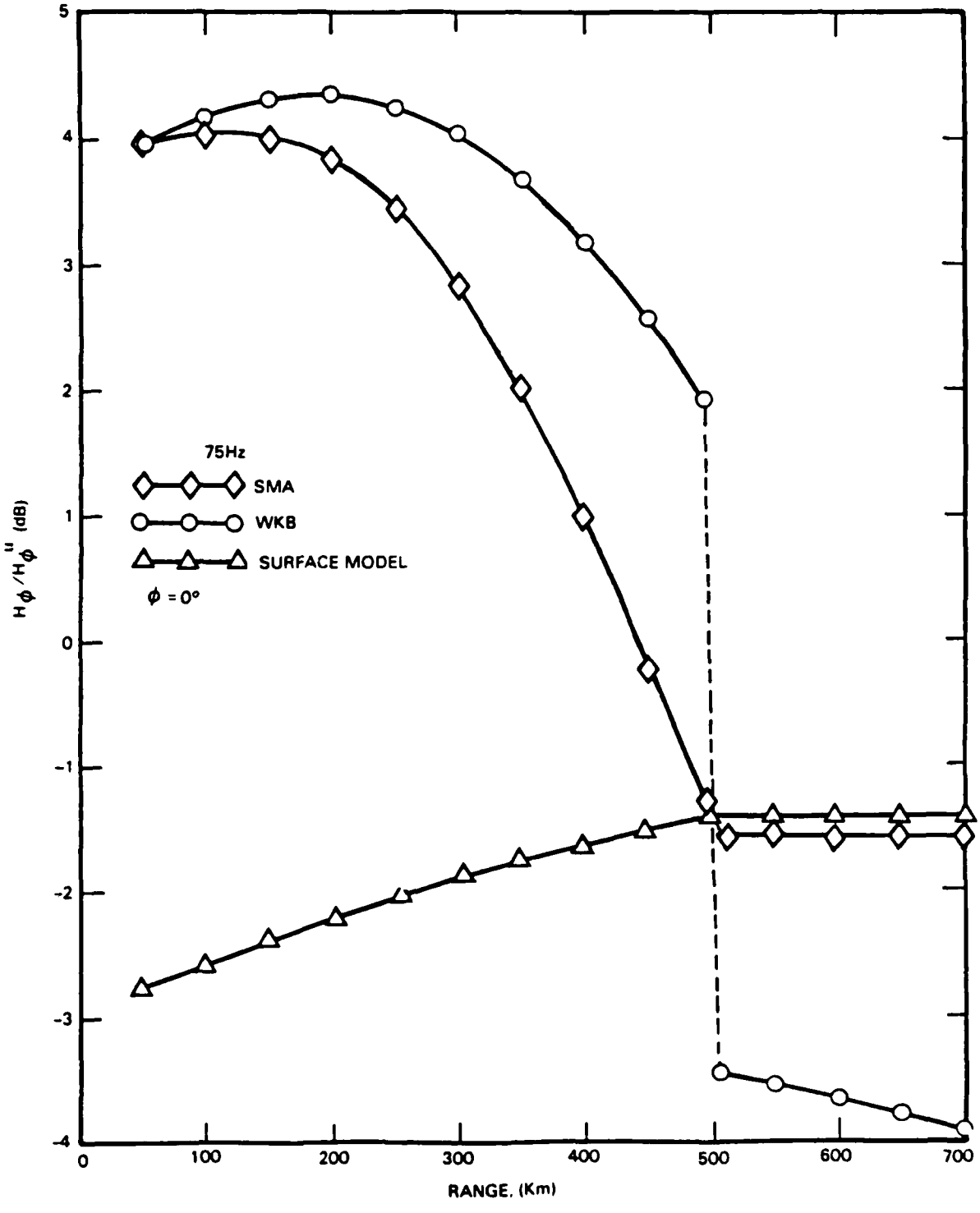

Figure 12. Ratio of disturbed to undisturbed H_ϕ in dB vs. range.

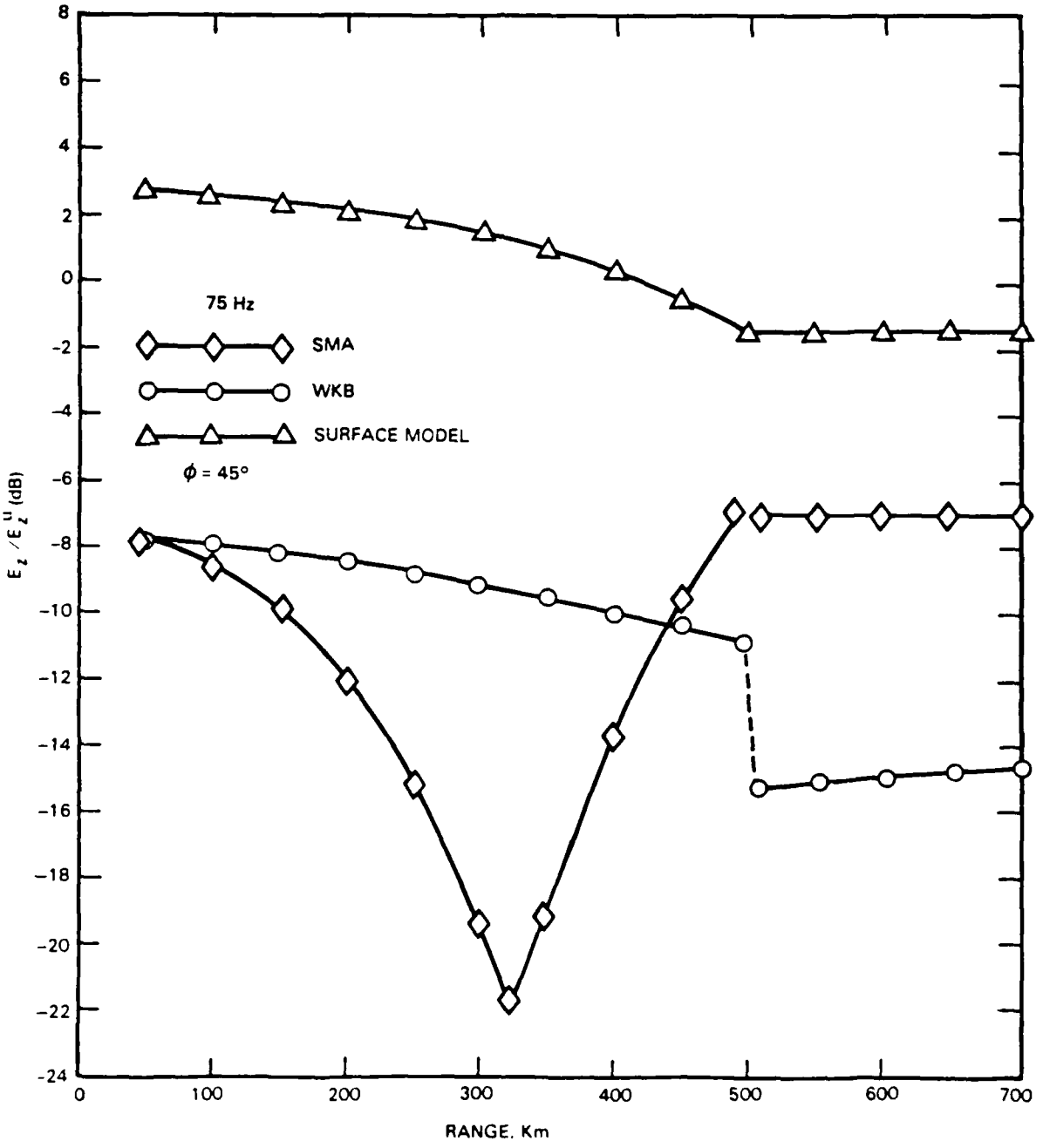

Figure 11. Ratio of disturbed to undisturbed E_z in dB vs. range.

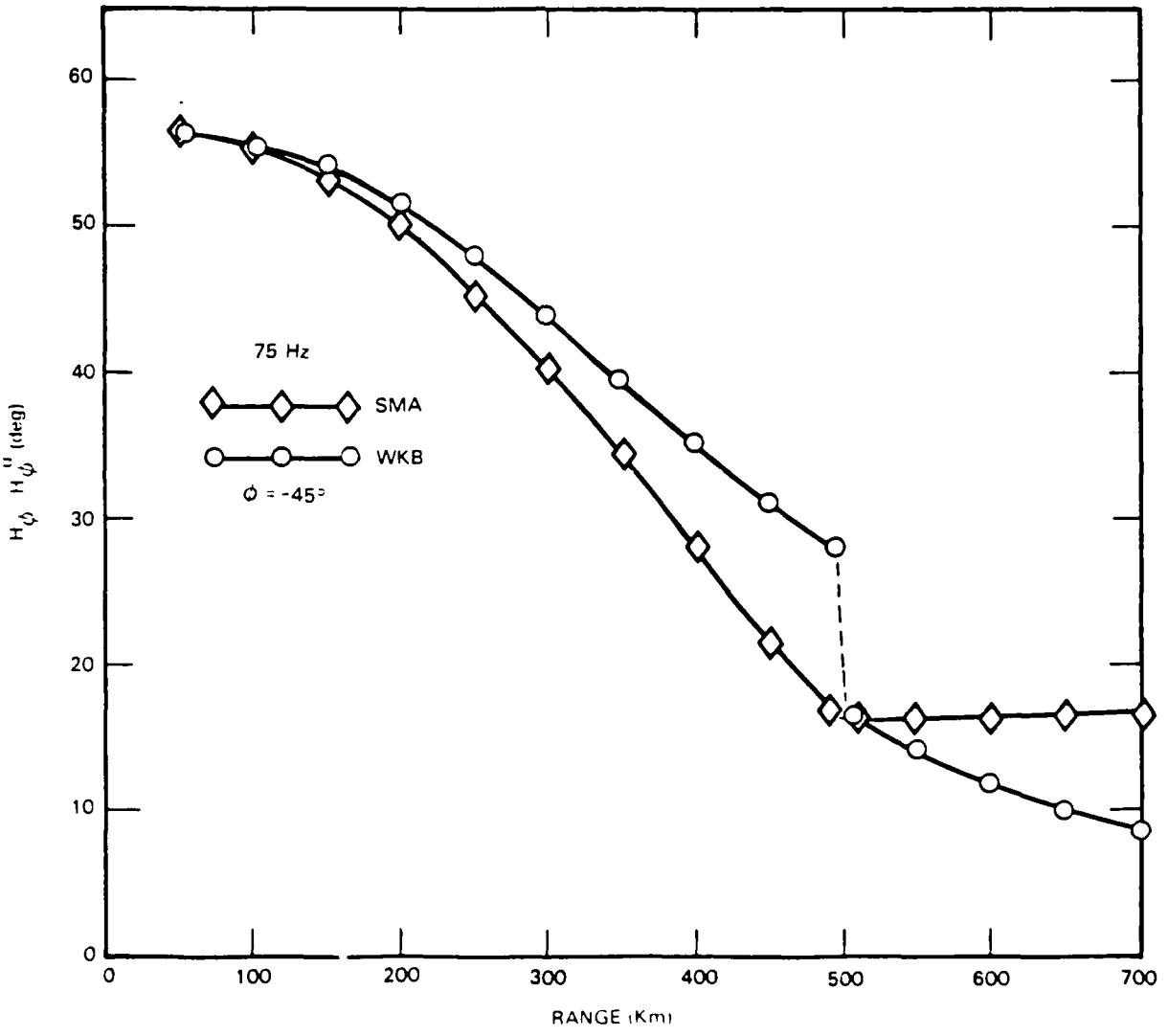

Figure 25. Disturbed and undisturbed phase difference for H_ϕ vs. range.

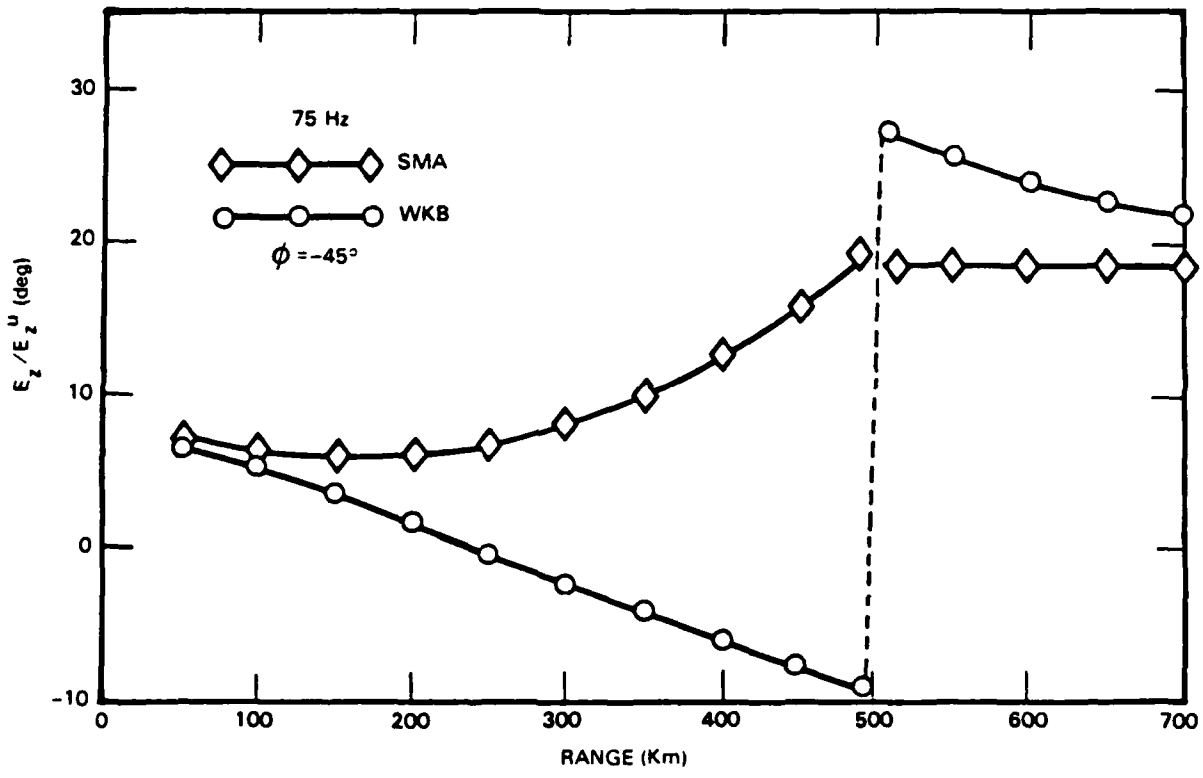

Figure 26. Disturbed and undisturbed phase difference for E_z vs. range.

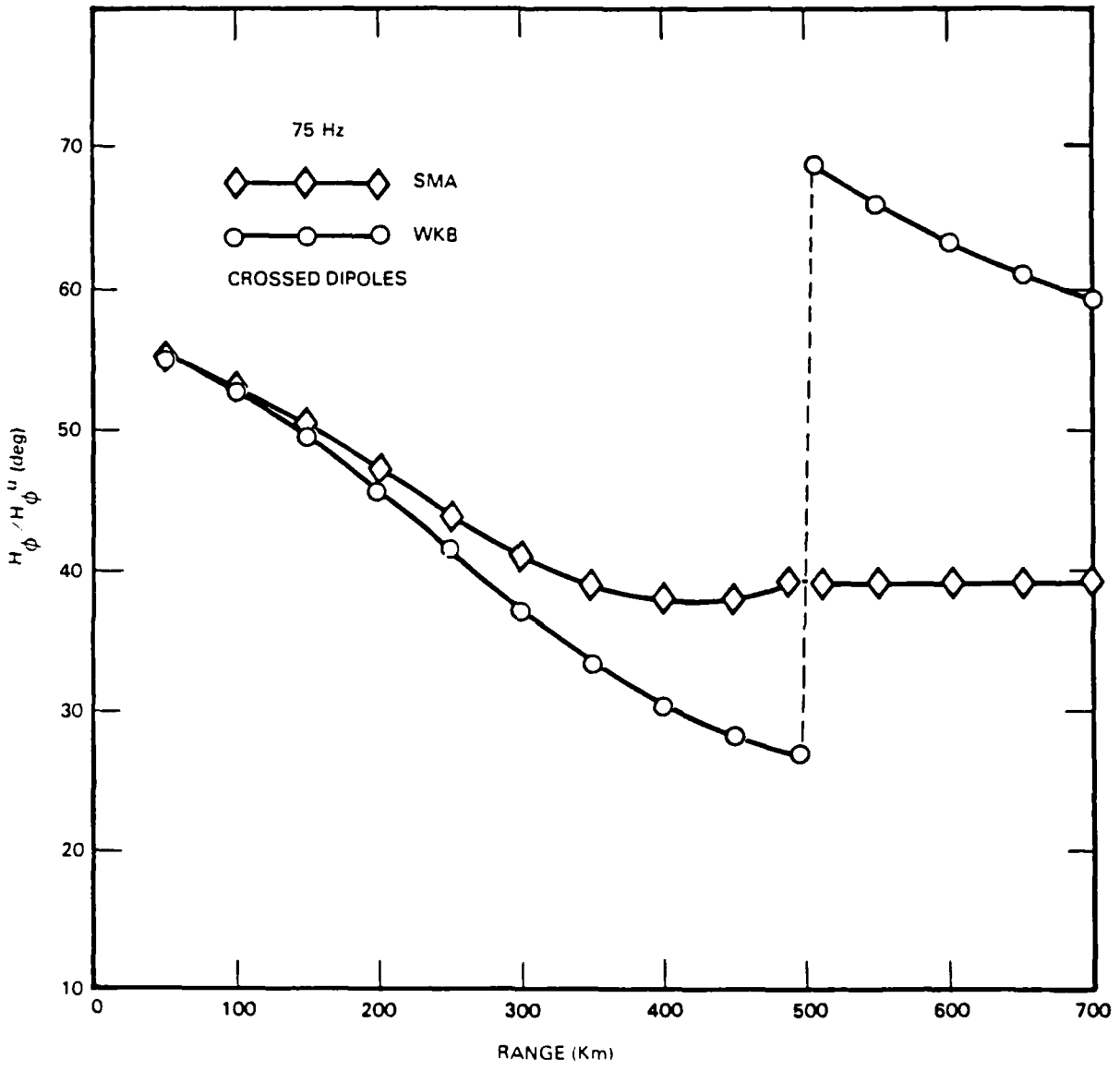

Figure 27. Disturbed and undisturbed phase difference for H_ϕ vs. range.

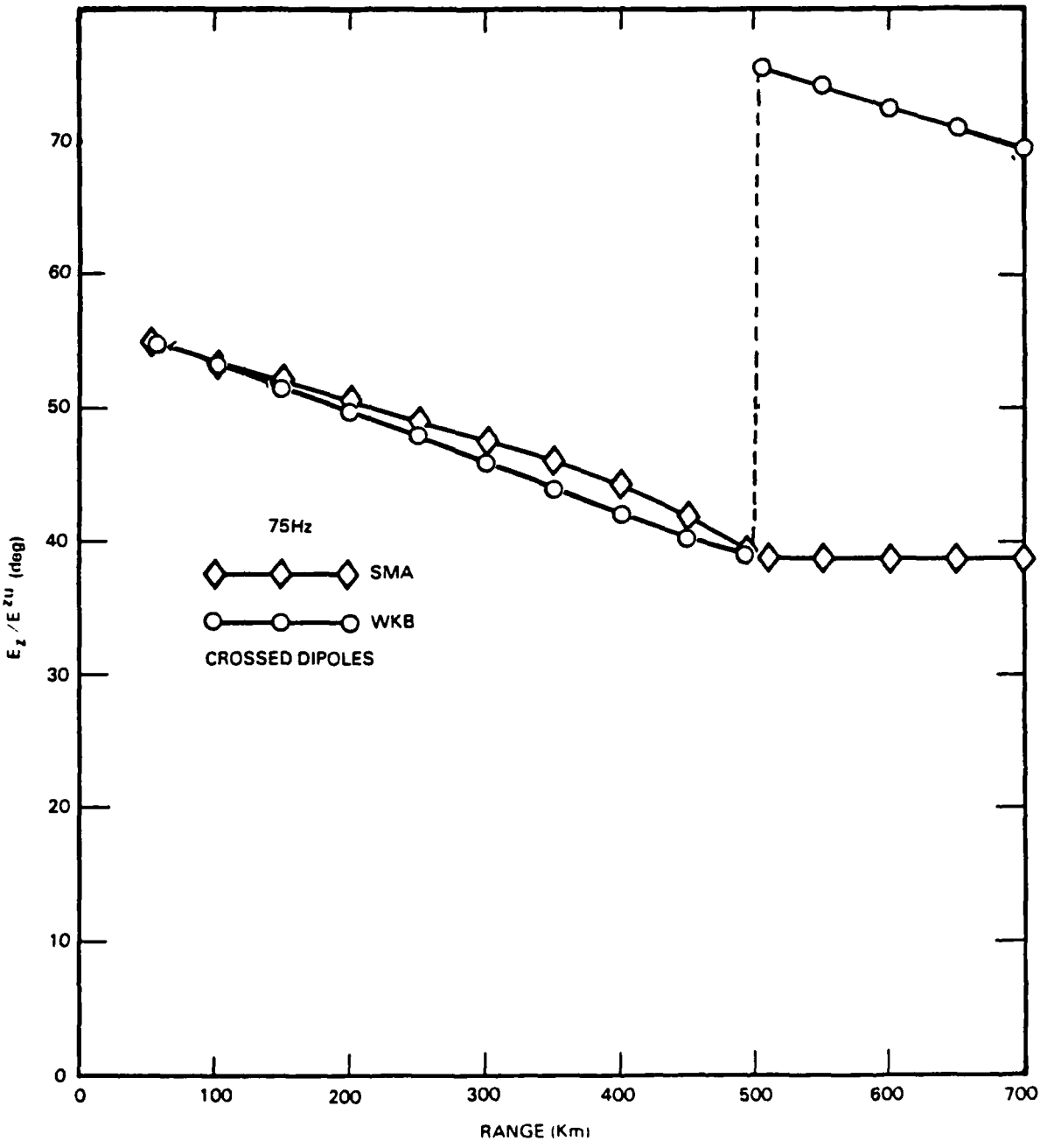

Figure 28. Disturbed and undisturbed phase difference for E_z vs. range.

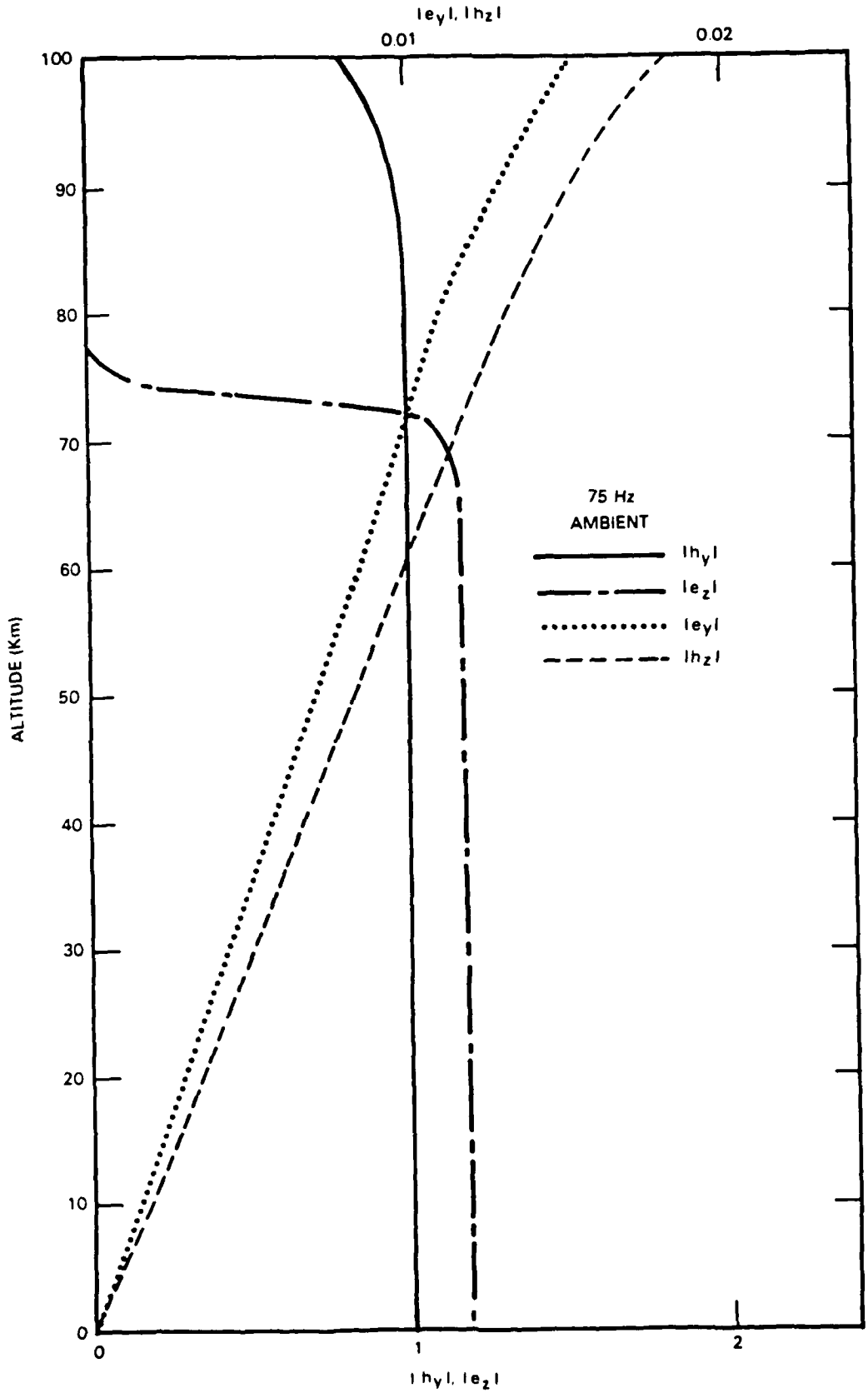

Figure 29. Height gain behavior for ambient guide.

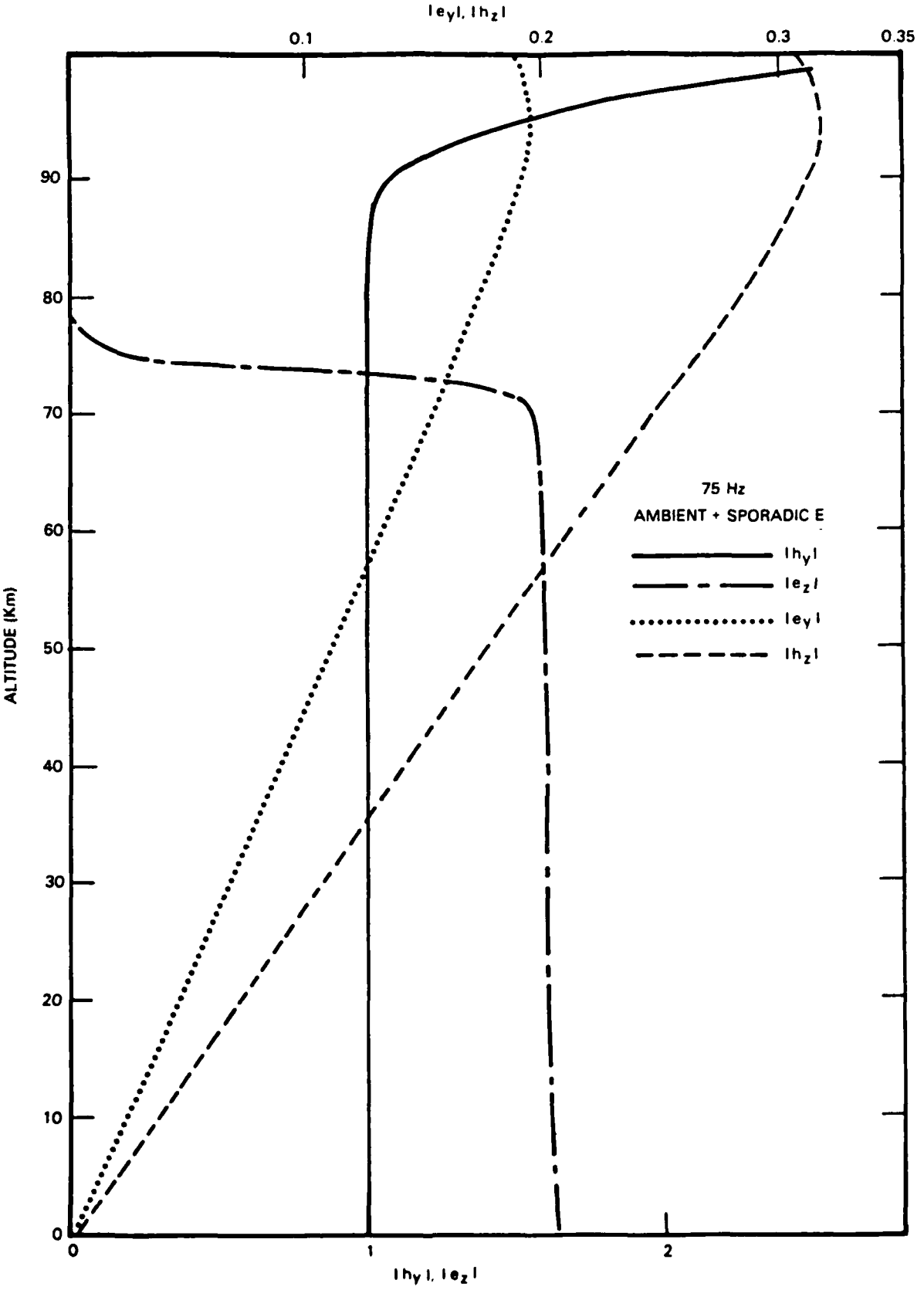

Figure 30. Height gain behavior for perturbed guide.

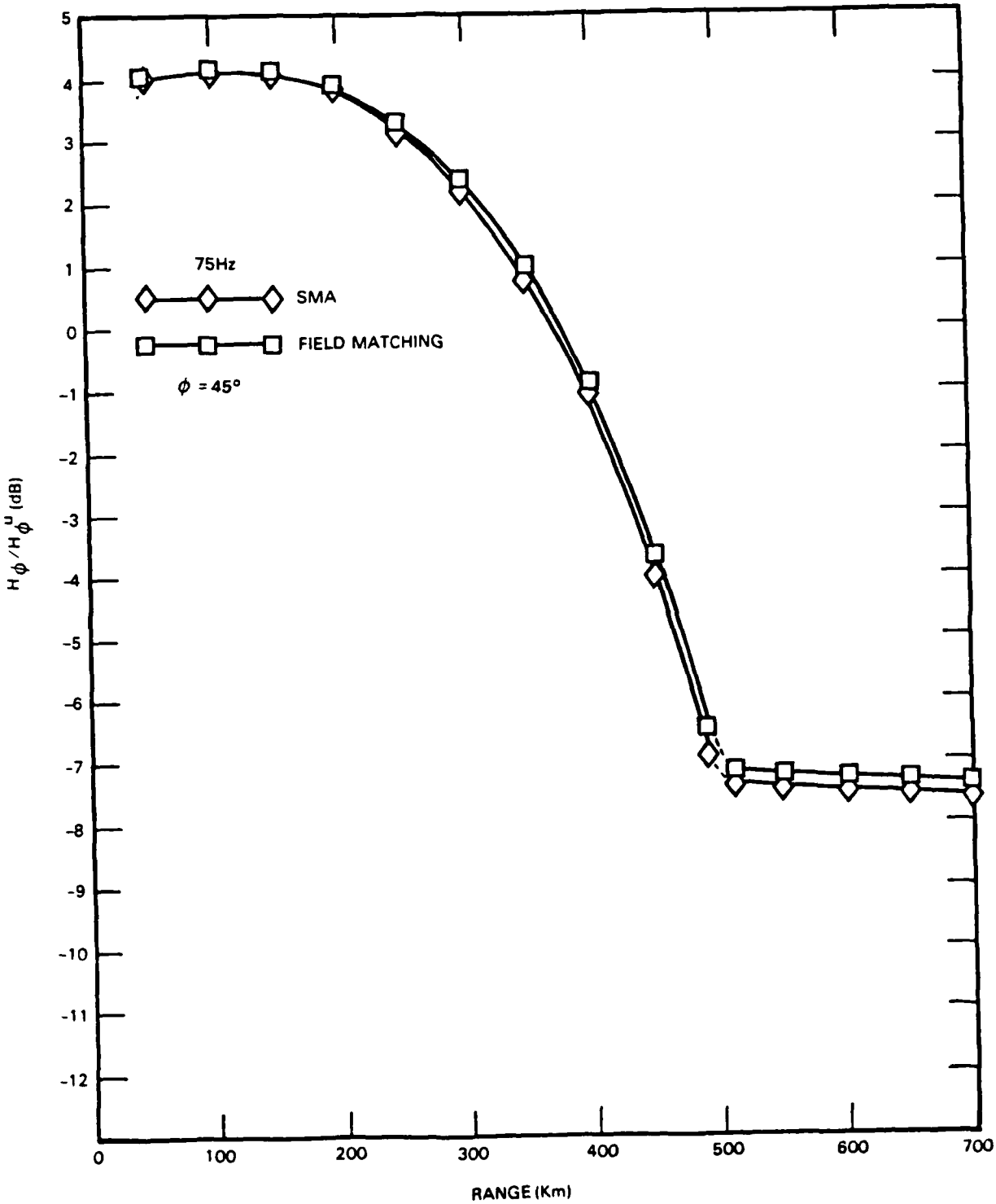

Figure 31. Comparison of SMA and Field Matching amplitudes for H_ϕ

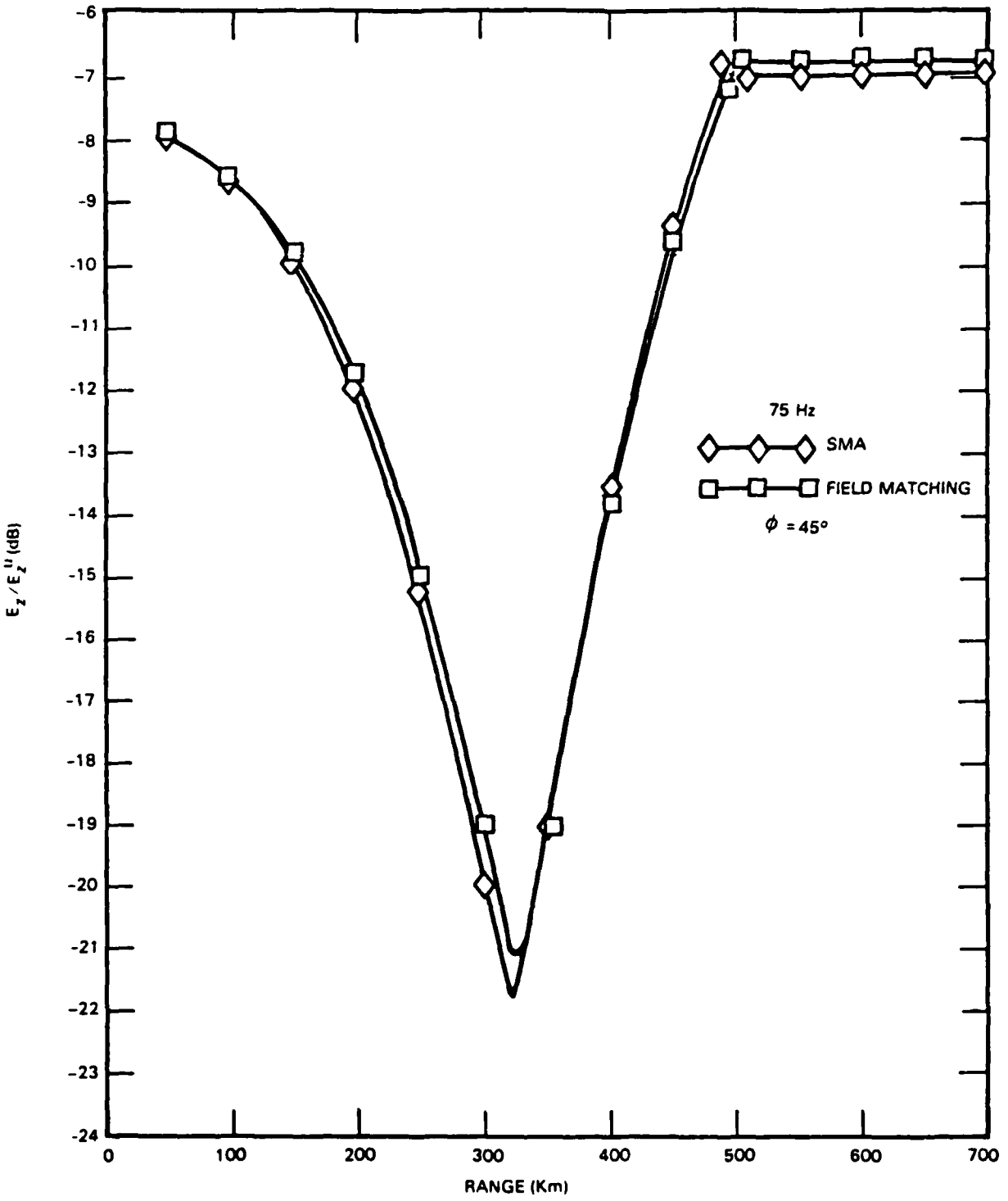

Figure 32. Comparison of SMA and Field Matching phases for E_z.

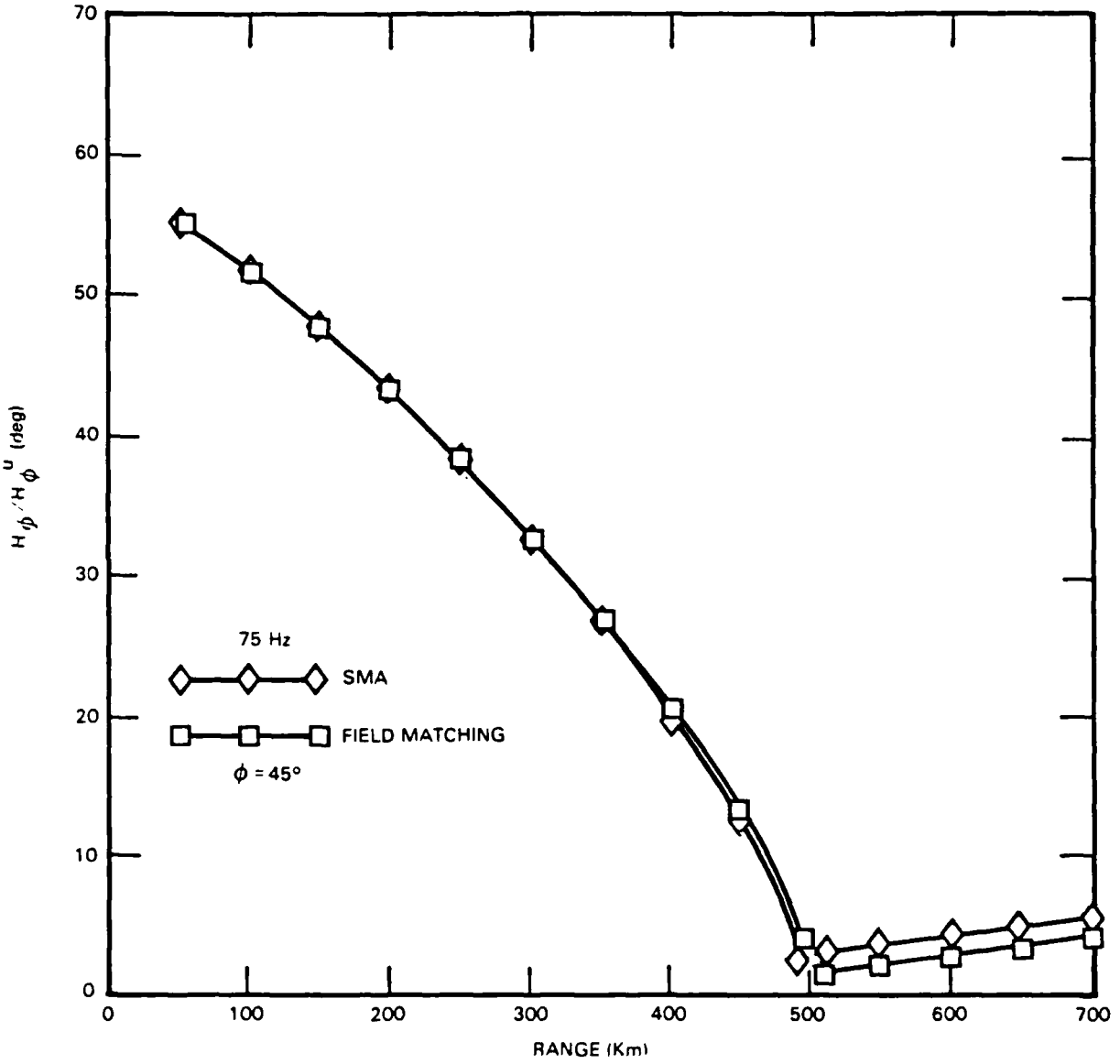

Figure 33. Comparison of SMA and Field Matching phases for H_ϕ

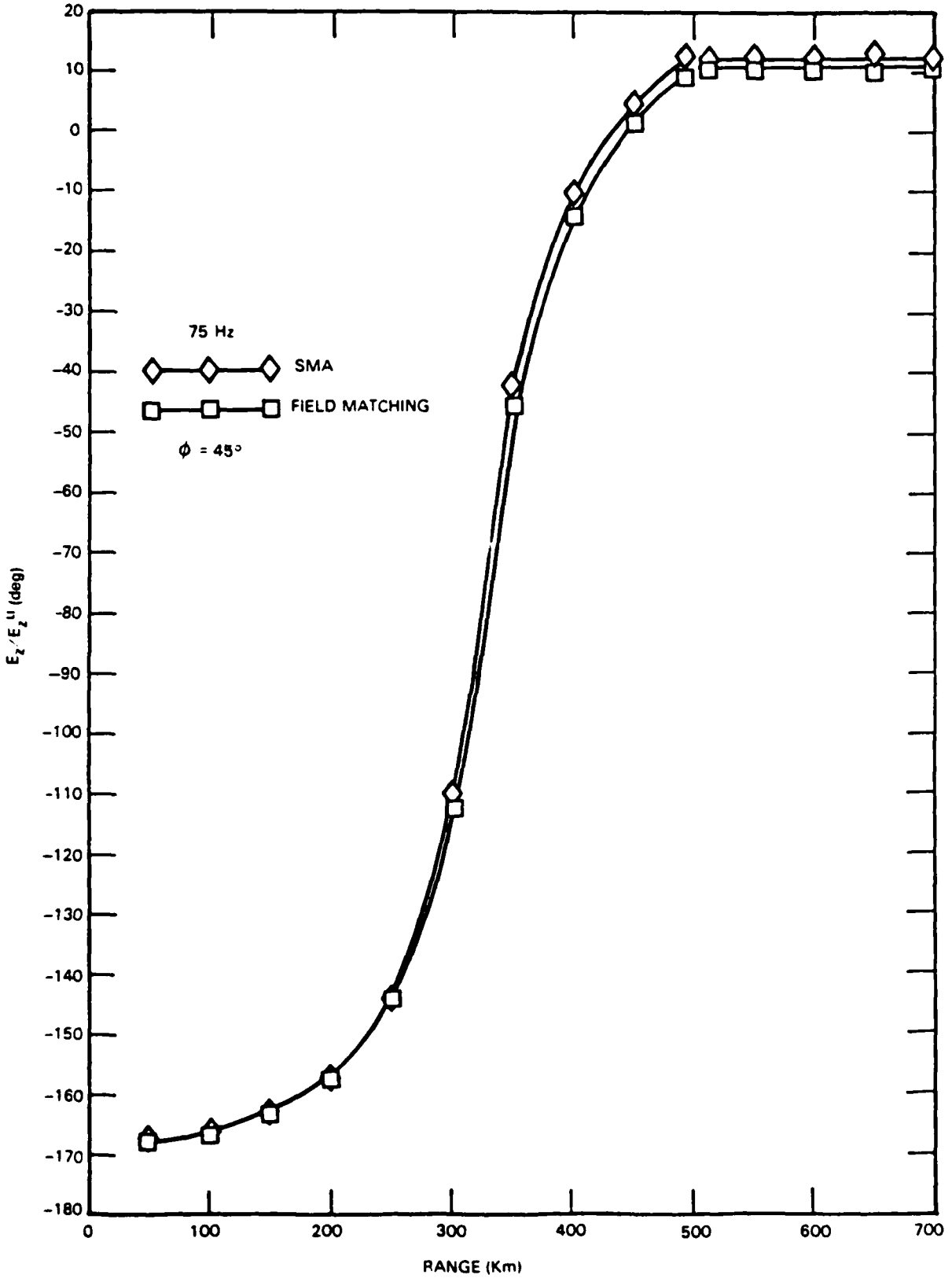

Figure 34. Comparison of SMA and Field Matching phases for E_z.

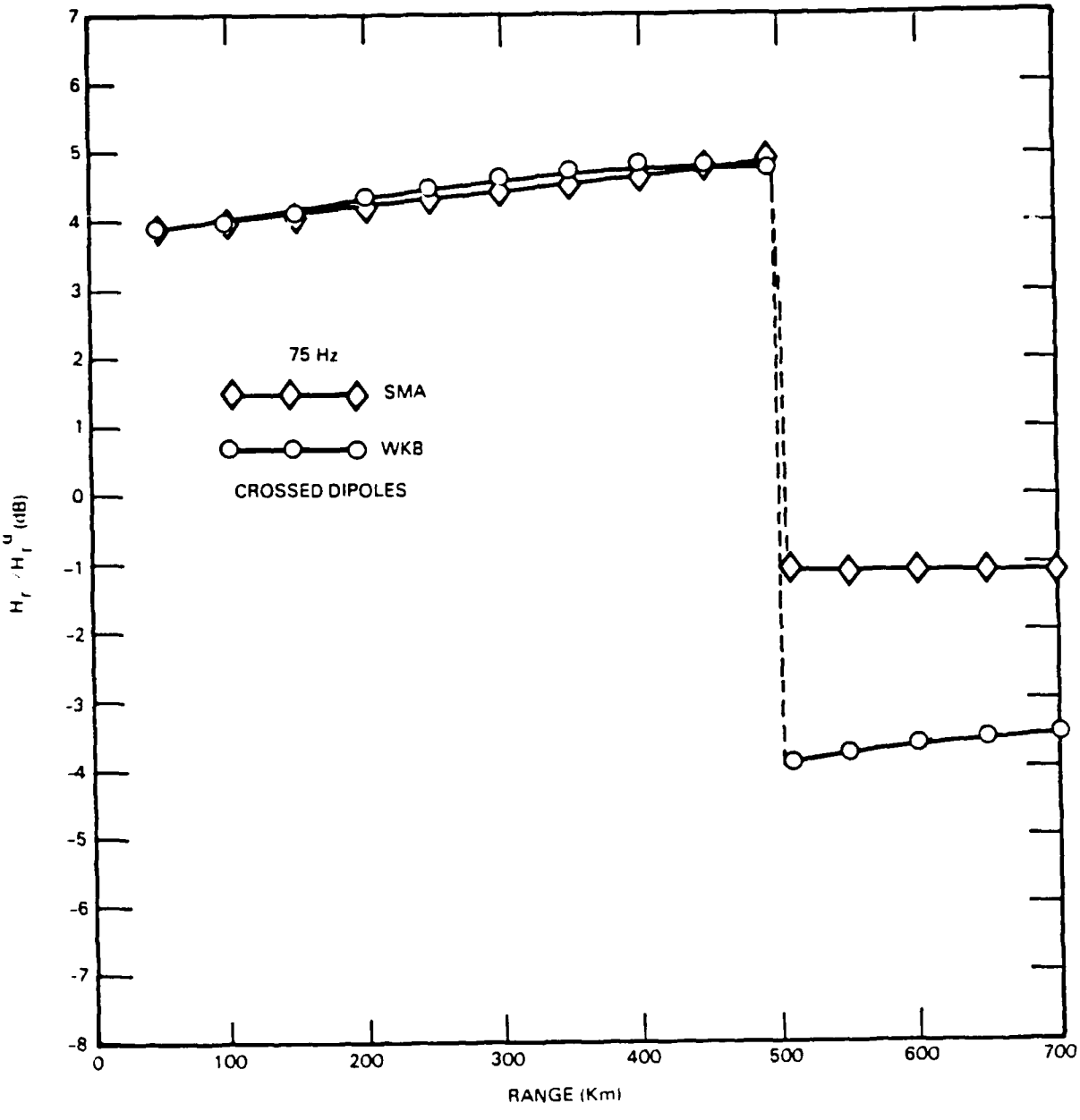

Figure 35. Ratio of disturbed to undisturbed H_r in dB vs. range.

DISTRIBUTION LIST

DEPARTMENT OF DEFENSE
DEPUTY UNDER SECRETARY OF DEFENSE
CMD, CONT, COMM & INTELL
DEPARTMENT OF DEFENSE
WASHINGTON, DC 20301

DIRECTOR
COMMAND CONTROL TECHNICAL CENTER
11440 ISAAC NEWTON SQUARE, N
RESTON, VA 22091
C-650

DIRECTOR
COMMAND CONTROL TECHNICAL CENTER
ROOM ME682, THE PENTAGON
WASHINGTON, DC 20301
C-312

DIRECTOR
DEFENSE ADVANCED RESEARCH PROJECT AGENCY
1440 WILSON BLVD
ARLINGTON, VA 22209
NUCLEAR MONITORING RSCH
STRATEGIC TECH OFFICE

DEFENSE COMMUNICATION ENGINEERING CENTER
1860 WIEHLE AVENUE
RESTON, VA 22090
CODE R220 (M HOROWITZ)
CODE R410
CODE R103

DIRECTOR
DEFENSE COMMUNICATIONS AGENCY
WASHINGTON, DC 20305
CODE 810
CODE 480
CODE 101B

DEFENSE COMMUNICATIONS AGENCY
WWMCCS SYSTEM ENGINEERING ORG
WASHINGTON, DC 20305
RL CRAWFORD

DEFENSE TECHNICAL INFORMATION CENTER
CAMERON STATION
ALEXANDRIA, VA 22314

DIRECTOR
DEFENSE INTELLIGENCE AGENCY
WASHINGTON, DC 20301
DIAST-5
DB-4C (EDWARD O'FARRELL)

DIRECTOR
DEFENSE NUCLEAR AGENCY
WASHINGTON, DC 20305
DDST
T:TL TECH LIBRARY
RAAE
STVL

DIRECTOR
JOINT STRAT TGT PLANNING STAFF JCS
OFFUTT AFB
OMAHA, NB 68113
JPST

COMMANDER
FIELD COMMAND
DEFENSE NUCLEAR AGENCY
KIRKTLAND AFB, NM 87115
FCPR

DIRECTOR INTERSERVICE NUCLEAR WEAPONS SCHOOL
KIRTLAND AFB, NM 87115
DOCUMENT CONTROL

CHIEF
LIVERMORE DIVISION FLD COMMAND DNA
LAWRENCE LIVERMORE LABORATORY
PO BOX 808
LIVERMORE, CA 94550
FCPRL

DIRECTOR
NATIONAL SECURITY AGENCY
FT GEORGE G MEADE, MD 20755
W65
OLIVER H BARTLETT W32
TECHNICAL LIBRARY
JOHN SKILLMAN R52

OJCS/J-3
THE PENTAGON
WASHINGTON, DC 20301
OPERATIONS (WWMCCS EVAL OFF, MR TOMA)

OJCS/J-5
THE PENTAGON
WASHINGTON, DC 20301
PLANS & POLICY (NUCLEAR DIVISION)

UNDER SECRY OF DEFENSE FOR RESEARCH AND ENGINEERING
DEPARTMENT OF DEFENSE
WASHINGTON, DC 20301
S&SS (OS)

DEPARTMENT OF THE ARMY
COMMANDER/DIRECTOR
ATMOSPHERIC SCIENCES LABORATORY
US ARMY ELECTRONICS COMMAND
WHITE SANDS MISSILE RANGE, NM 88002
DELAS-AE-M (FE NILES)

COMMANDER
HARRY DIAMOND LABORATORIES
2800 POWDER MILL RD
ADELPHI, MD 20783
DELHD-NP (FN WIMENITZ)
MILDRED H WEINER DRXDO-II

COMMANDER
US ARMY FOREIGN SCIENCE & TECH CENTER
220 7TH STREET, NE
CHARLOTTESVILLE, VA 22901
R JONES
PA CROWLEY

COMMANDER
US ARMY NUCLEAR AGENCY
7500 BACKLICK ROAD
BUILDING 2073
SPRINGFIELD, VA 22150
MONA-WE (J BERBERET)

CHIEF
US ARMY RESEARCH OFFICE
PO BOX 12211
TRIANGEL PARK, NC 27709
DRXRD-ZC

DEPARTMENT OF THE NAVY
CHIEF OF NAVAL OPERATIONS
NAVY DEPARTMENT
WASHINGTON, DC 20350
OP 941
OP 604C3
OP 943
OP 981

CHIEF OF NAVAL RESEARCH
NAVY DEPARTMENT
ARLINGTON, VA 22217
CODE 402
CODE 420
CODE 421
CODE 461
CODE 464

COMMANDING OFFICER
NAVAL INTELLIGENCE SUPPORT CENTER
4301 SUITLAND RD BLDG 5
WASHINGTON, DC 20390

OFFICER-IN-CHARGE
WHITE OAK LABORATORY
NAVAL SURFACE WEAPONS CENTER
SILVER SPRING, MD 20910
CODE WA501 NAVY NUC PRGMS OFF
CODE WX21 TECH LIBRARY

COMMANDER
NAVAL TELECOMMUNICATIONS COMMAND
NAVTELCOM HEADQUARTERS
4401 MASSACHUSETTS AVE, NW
WASHINGTON, DC 20390
CODE 24C

COMMANDING OFFICER
NAVY UNDERWATER SOUND LABORATORY
FORT TRUMBULL
NEW LONDON, CT 06320
PETER BANNISTER
DA MILLER

DIRECTOR
STRATEGIC SYSTEMS PROJECT OFFICE
NAVY DEPARTMENT
WASHINGTON, DC 20376
N141

DEPARTMENT OF THE AIR FORCE
COMMANDER
ADC/DC
ENT AFB, CO 80912
DC (MR LONG)

COMMANDER
ADCOM/XPD
ENT AFB, CO 80912
XPQDQ
XP

AF GEOPHYSICS LABORATORY, AFSC
HASCOM AFB, MA 01731
CRU (S HOROWITZ)

AF WEAPONS LABORATORY, AFSC
KIRTLAND AFB, NM 87117
SUL (2)
DYC

COMMANDER
ROME AIR DEVELOPMENT CENTER, AFSC
GRIFFISS AFB, NY 13440
EMTLD DOC LIBRARY

COMMANDER
ROME AIR DEVELOPMENT CENTER, AFSC
HANSCOM AFB, MA 01731
EEP JOHN RASMUSSEN

COMMANDER IN CHIEF
STRATEGIC AIR COMMAND
OFFUTT AFB, NB 68113
NRT
XPFS

LAWRENCE LIVERMORE NATIONAL
LABORATORY
PO BOX 808
LIVERMORE, CA 94550
TECH INFO DEPT L-3

LOS ALAMOS NATIONAL SCIENTIFIC
LABORATORY
PO BOX 1663
LOS ALAMOS, NM 87545
DOC CON FOR TF TASCHEK
DOC CON FOR D R WESTERVELT
DOC CON FOR PW KEATON

SANDIA LABORATORY
LIVERMORE NATIONAL LABORATORY
PO BOX 969
LIVERMORE, CA 94550
DOC CON FOR BE MURPHEY
DOC CON FOR TB COOK ORG 8000

SANDIA NATIONAL LABORATORY
PO BOX 5800
ALBUQUERQUE, NM 87115
DOC CON FOR SPACE PROJ DIV
DOC CON FOR AD THORNBROUGH
DOC CON FOR 3141 SANDIA RPT COLL

OTHER GOVERNMENT
DEPARTMENT OF COMMERCE
NATIONAL BUREAU OF STANDARDS
WASHINGTON, DC 20234
RAYMOND T MOORE

DEPARTMENT OF COMMERCE
OFFICE OF TELECOMMUNICATIONS
INSTITUTE FOR TELECOM SCIENCE
BOULDER, CO 80302
WILLIAM F UTLAUT
LA BERRY
A GLENN JEAN

DEPARTMENT OF DEFENSE CONTRACTORS
AEROSPACE CORPORATION
PO BOX 92957
LOS ANGELES, CA 90009
IRVING M GARFUNKEL

ANALYTICAL SYSTEMS ENGINEERING CORP
5 OLD CONCORD RD
BURLINGTON, MA 01803
RADIO SCIENCES

THE BOEING COMPANY
PO BOX 3707
SEATTLE, WA 98124
GLENN A HALL
JF KENNEY

ESL, INC
495 JAVA DRIVE
SUNNYVALE, CA 94086
JAMES MARSHALL

GENERAL ELECTRIC COMPANY
SPACE DIVISION
VALLEY FORGE SPACE CENTER
GODDARD BLVD KING OF PRUSSIA
PO BOX 8555
PHILADELPHIA, PA 19101
SPACE SCIENCE LAB (MH BORTNER)

KAMAN TEMPO
816 STATE STREET
PO DRAWER QQ
SANTA BARBARA, CA 93102
B GAMBILL
DASIAC
WARREN S KNAPP

GTE SYLVANIA, INC
ELECTRONICS SYSTEMS GRP
EASTERN DIVISION
77 A STREET
NEEDHAM, MA 02194
MARSHAL CROSS

ITT RESEARCH INSTITUTE
10 WEST 35TH STREET
CHICAGO, IL 60616
TECHNICAL LIBRARY

UNIVERSITY OF ILLINOIS
DEPARTMENT OF ELECTRICAL ENGINEERING
URBANA, IL 61803
AERONOMY LABORATORY

JOHNS HOPKINS UNIVERSITY
APPLIED PHYSICS LABORATORY
JOHNS HOPKINS ROAD
LAUREL, MD 20810
J NEWLAND
PT KOMISKE

LOCKHEED MISSILE & SPACE CO, INC
3251 HANOVER STREET
PALO ALTO, CA 94304
EE GAINES
WL IMHOF D/52-12
JB REAGAN D652-12
RG JOHNSON D/52-12

MASSACHUSETTS INSTITUTE OF TECHNOLOGY
LINCOLN LABORATORY
PO BOX 73
LEXINGTON, MA 02173
DM TOWLE

MISSION RESEARCH CORPORATION
735 STATE STREET
SANTA BARBARA, CA 93101
R HENDRICK
F FAJEN

MITRE CORPORATION
PO BOX 209
BEDFORD, MA 01730
G HARDING

PACIFIC-SIERRA RESEARCH CORP
1456 CLOVERFIELD BLVD
SANTA MONICA, CA 90404
EC FIELD, JR

PENNSYLVANIA STATE UNIVERSITY
IONOSPHERIC RESEARCH LABORATORY
318 ELECTRICAL ENGINEERING EAST
UNIVERSITY PARK, PA 16802
IONOSPHERIC RSCH LAB

R&D ASSOCIATES
PO BOX 9695
MARINA DEL REY, CA 90291
FORREST GILMORE
WILLIAM J KARZAS
PHYLLIS GREIFINGER
CARL GREIFINGER
HA ORY
BRYAN GABBARD
RP TURCO
SAUL ALTSCHULER

RAND CORPORATION
1700 MAIN STREET
SANTA MONICA, CA 90406
TECHNICAL LIBRARY
CULLEN CRAIN

SRI INTERNATIONAL
333 RAVENSWOOD AVENUE
MENLO PARK, CA 94025
DONALD NEILSON
GEORGE CARPENTER
WG CHETNUT
JR PETERSON
GARY PRICE

STANFORD UNIVERSITY
RADIO SCIENCE LABORATORY
STANFORD, CA 94305
RA HELLIWELL
FRASER SMITH
J KATSUFRAKIS

CALIFORNIA INSTITUTE OF TECHNOLOGY
JET PROPULSION LABORATORY
4800 OAK GROVE DRIVE
PASADENA, CA 91103
ERNEST K SMITH

END

FILMED

11-85

DTIC